Inorganic Chemistry

Article

pubs.acs.org/IC

Exploring the Influence of Diamagnetic Ions on the Mechanism of Magnetization Relaxation in $\{Co^{III}_2Ln^{III}_2\}$ (Ln = Dy, Tb, Ho) "Butterfly" Complexes

Kuduva R. Vignesh,[†] Stuart K. Langley,[‡] Keith S. Murray,*[,§] and Gopalan Rajaraman*[,∥]

[†]IITB-Monash Research Academy, Indian Institute of Technology Bombay, Powai, Mumbai 400076, India

[‡]School of Science and the Environment, Division of Chemistry, Manchester Metropolitan University, Manchester M15 6HB, U. K.

[§]School of Chemistry, Monash University, Clayton, Victoria 3800, Australia

[∥]Department of Chemistry, Indian Institute of Technology Bombay, Powai, Mumbai 400076, India

Supporting Information

ABSTRACT: The synthesis and magnetic and theoretical studies of three isostructural heterometallic $[Co^{III}_2Ln^{III}_2(\mu_3\text{-}OH)_2(o\text{-tol})_4(mdea)_2(NO_3)_2]$ (Ln = Dy (**1**), Tb (**2**), Ho (**3**)) "butterfly" complexes are reported (*o*-tol = *o*-toluate, $(mdea)^{2-}$ = doubly deprotonated *N*-methyldiethanolamine). The Co^{III} ions are diamagnetic in these complexes. Analysis of the dc magnetic susceptibility measurements reveal antiferromagnetic exchange coupling between the two Ln^{III} ions for all three complexes. ac magnetic susceptibility measurements reveal single-molecule magnet (SMM) behavior for complex **1**, in the absence of an external magnetic field, with an anisotropy barrier U_{eff} of 81.2 cm^{-1}, while complexes **2** and **3** exhibit field induced SMM behavior, with a U_{eff} value of 34.2 cm^{-1} for **2**. The barrier height for **3** could not be quantified. To understand the experimental observations, we performed DFT and ab initio CASSCF+RASSI-SO calculations to probe the single-ion properties and the nature and magnitude of the Ln^{III}–Ln^{III} magnetic coupling and to develop an understanding of the role the diamagnetic Co^{III} ion plays in the magnetization relaxation. The calculations were able to rationalize the experimental relaxation data for all complexes and strongly suggest that the Co^{III} ion is integral to the observation of SMM behavior in these systems. Thus, we explored further the effect that the diamagnetic Co^{III} ions have on the magnetization blocking of **1**. We did this by modeling a dinuclear $\{Dy^{III}_2\}$ complex (**1a**), with the removal of the diamagnetic ions, and three complexes of the types $\{K^{I}_2Dy^{III}_2\}$ (**1b**), $\{Zn^{II}_2Dy^{III}_2\}$ (**1c**), and $\{Ti^{IV}_2Dy^{III}_2\}$ (**1d**), each containing a different diamagnetic ion. We found that the presence of the diamagnetic ions results in larger negative charges on the bridging hydroxides (**1b** > **1c** > **1** > **1d**), in comparison to **1a** (no diamagnetic ion), which reduces quantum tunneling of magnetization effects, allowing for more desirable SMM characteristics. The results indicate very strong dependence of diamagnetic ions in the magnetization blocking and the magnitude of the energy barriers. Here we propose a synthetic strategy to enhance the energy barrier in lanthanide-based SMMs by incorporating s- and d-block diamagnetic ions. The presented strategy is likely to have implications beyond the single-molecule magnets studied here.

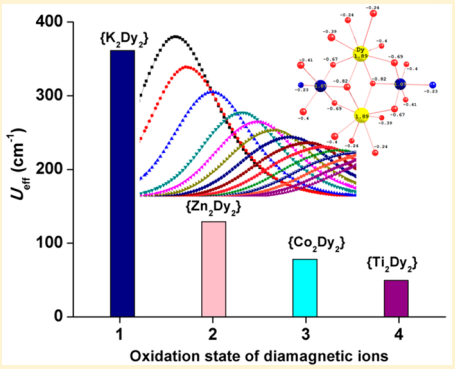

INTRODUCTION

Lanthanide ions have begun to overshadow d-block transition metals in the development of new molecular magnetic materials, such as single-molecule magnets (SMMs).[1] Primarily, the trivalent ions of dysprosium and terbium have been extensively used in the syntheses of new SMMs[2] because of the strong anisotropy provided by these ions.[3] SMM behavior has generated great interest due to the physical properties linked with magnetic hysteresis and quantum tunneling of magnetization (QTM), with potential applications in high-density information storage devices,[4] as Qubits[5] and "Spintronic" devices.[5a,6] The great shift toward lanthanide-based SMMs is a result of the observation of extremely large anisotropy barriers,[7] the magnitudes of which are significantly larger than what has previously been observed for polynuclear 3d clusters.[6,8] The anisotropy barrier (U_{eff}) is the energy required to "flip" the orientation of the magnetic moment and return to thermal equilibrium in the ground magnetic microstates. With such large energy barriers, one would expect to store digital information at temperatures much greater than those currently possible (blocking temperatures of 14 and 30 K[9,10]); however, this has not materialized due to fast QTM which shortcuts the barrier, resulting in "fast" magnetization reversal. Most lanthanide-based SMMs reported in the literature use Dy^{III} and Tb^{III} because these ions have a large magnetic anisotropy and a lower tendency to exhibit QTM, in comparison to other lanthanide ions. To limit QTM further, strong magnetic

Received: November 9, 2016
Published: February 17, 2017

Downloaded via INDIAN INST OF TECHNOLOGY BOMBAY on October 20, 2020 at 13:57:07 (UTC).
See https://pubs.acs.org/sharingguidelines for options on how to legitimately share published articles.

© 2017 American Chemical Society

DOI: 10.1021/acs.inorgchem.6b02720
Inorg. Chem. 2017, 56, 2518–2532

exchange interactions between polynuclear 4f complexes are favorable and/or the synthesis of 4f single ion sites which display an Ising type magnetic anisotropy, with a minimal transverse component. A representative example of the former, a $\{Tb_2\}$ complex, displays a U_{eff} value of 226 cm^{-1} and magnetic hysteresis up to temperatures as high as 14 K,[9a] while an example of the latter is the report of a pseudo-D_{5h}-symmetry Dy^{III} complex exhibiting very large magnetic blocking temperatures and negligible transverse terms in both the ground and the first excited states.[10]

Recently, heterometallic 3d/4f complexes have been actively studied as an alternative to pure 4f coordination complexes. This area of active research has arisen from recent experimental data which indicate that two separate synthetic strategies can be considered. The first approach uses paramagnetic 3d transition-metal ions, taking advantage of the combination of the large spin of 3d ions with the spin/anisotropy of the 4f ions.[11] More importantly, the 3d ions offer the potential to provide stronger magnetic exchange interactions than are possible for pure polynuclear 4f complexes. Such 3d−4f magnetic exchange interactions have been shown to significantly reduce QTM, and using 3d ions such as Cr^{III},[12] Fe^{III},[13] Mn^{III},[14] and Ni^{II} [15] have provided heterometallic 3d−4f SMMs with long relaxation times (>100 s) up to 4.7 K.[12a] The second approach utilizes diamagnetic ions in conjunction with Ln^{III} ions. It has been shown that these cations influence the electron density distribution of surrounding coordinating ligands, thus affecting the electronic structure and the single-ion magnet properties of the Ln^{III} ion. Systems such as $\{Zn^{II}Dy^{III}\}$[16] have provided clear evidence that positively charged diamagnetic ions can help stabilize an Ising-type anisotropy for the 4f ion. This strategy has successfully been employed toward the isolation of several Dy^{III} SMMs with attractive barrier heights.[16]

On the basis of the diamagnetic ion approach, one can assume that the Co^{III} ion with a low-spin d^6 electron configuration is an ideal candidate to stabilize heterometallic 3d−4f complexes, containing a highly charged diamagnetic ion. Some of us have already reported a family of tetranuclear $\{Co^{III}_2Ln^{III}_2\}$ SMMs, where the SMM behavior is influenced by the ligand environment surrounding the Dy^{III} ion. The energy barrier in these complexes were found to range from 14 to 170 K depending on the ligands utilized in the synthesis of each complex.[17] Previous studies on these systems focused heavily on the effect of the ligand; however, no studies have been made to probe the influence/importance of the diamagnetic ion on these SMMs, and in particular how the relaxation can be affected by different diamagnetic ions. In this report we have synthesized a new family of heterometallic $\{Co^{III}_2Ln^{III}_2\}$ (Ln = Tb, Dy, Ho) complexes using the ligands *N*-methyldiethanolamine ($mdeaH_2$) and *o*-toluic acid (*o*-tolH). The complexes are of general formula $[Co^{III}_2Ln^{III}_2(\mu_3\text{-}OH)_2(o\text{-}tol)_4(mdea)_2(NO_3)_2]$ (Ln = Dy (**1**), Tb (**2**), Ho (**3**)), each containing a diamagnetic Co^{III} ion. We report the synthesis and magnetic properties, provide an ab initio and density functional theory (DFT) theoretical description of the three complexes, and explore the effect the diamagnetic Co^{III} ion has on the energy barrier to magnetic reversal.

EXPERIMENTAL SECTION

General Information. All reactions were carried out under aerobic conditions. Chemicals and solvents were obtained from commercial sources and used without further purification.

Synthesis of $[Co^{III}_2Dy^{III}_2(\mu_3\text{-}OH)_2(o\text{-}tol)_4(mdea)_2(NO_3)_2]$ (1). $Co(NO_3)_2{\cdot}6H_2O$ (0.29 g, 1 mmol) and $Dy(NO_3)_3{\cdot}6H_2O$ (0.22 g, 0.5 mmol) were dissolved in MeCN (20 mL), followed by the addition of *N*-methyldiethanolamine (0.1 mL, 1 mmol), *o*-toluic acid (0.14 g, 1.0 mmol), and triethylamine (0.55 mL, 4.0 mmol), which resulted in a dark green solution. This solution was stirred for 4 h, after which the solvent was removed, resulting in a green oil. The oil was redissolved in MeOH/^{i}PrOH (1/1) and layered with diethyl ether (Et_2O). Within 8−10 days, green crystals of **1** had appeared, in approximate yield of 65% (crystalline product). Anal. Calcd (found) for $Co_2Dy_2C_{42}H_{52}N_4O_{20}$: C, 36.67 (36.86); H, 3.81 (3.86); N, 4.07 (4.32).

Synthesis of $[Co^{III}_2Tb^{III}_2(\mu_3\text{-}OH)_2(o\text{-}tol)_4(mdea)_2(NO_3)_2]$ (2). The synthesis for **1** was followed, but $Tb(NO_3)_3{\cdot}6H_2O$ (0.17 g, 0.5 mmol) was used in place of $Dy(NO_3)_3{\cdot}6H_2O$. Dark green crystals of **2** appeared within 10−15 days, in an approximate yield of 47% (crystalline product). Anal. Calcd (found) for $Co_2Tb_2C_{42}H_{52}N_4O_{20}$: C, 36.86 (36.34); H, 3.83 (3.67); N, 4.09 (4.23).

Synthesis of $[Co^{III}_2Ho^{III}_2(\mu_3\text{-}OH)_2(o\text{-}tol)_4(mdea)_2(NO_3)_2]$ (3). The synthesis for **1** was followed, but $Ho(NO_3)_3{\cdot}6H_2O$ (0.22 g, 0.5 mmol) was used in place of $Dy(NO_3)_3{\cdot}6H_2O$. Dark green crystals of **3** appeared within 10−12 days, in an approximate yield of 52% (crystalline product). Anal. Calcd (found) for $Co_2Ho_2C_{42}H_{52}N_4O_{20}$: C, 36.53 (36.71); H, 3.80 (3.93); N, 4.06 (4.11).

X-ray Crystallography. Single-crystal X-ray diffraction measurements for **1** and **2** were performed at 100(2) K at the Australian synchrotron MX1 beamline.[18] Data collection and integration were performed with Blu-Ice[19] and XDS[20] software programs. Compounds **1** and **2** were solved by direct methods (SHELXS-97)[21] and refined (SHELXL-97)[22] by full least-matrix least-squares on all F^2 data.[23] Crystallographic data and refinement parameters for **1** and **2** are summarized in Table S1 in the Supporting Information. CCDC numbers 1510217 (**1**) and 1510218 (**2**) contain crystallographic data; these data can be obtained free of charge from the Cambridge Crystallographic Data Centre via www.ccdc.cam.ac.uk/data_request/cif. Powder X-ray diffraction measurements were performed for complex **3** and were measured on a Bruker X8 Focus powder diffractometer using the Cu Kα wavelength (1.5418 Å). The samples were mounted on a zero-background silicon single-crystal stage. Scans were performed at room temperature in the 2θ range 5−55° and compared with predicted patterns on the basis of low-temperature single-crystal data.

Magnetic Measurements. Magnetic susceptibility measurements were carried out on a Quantum Design MPMS-XL 7 SQUID magnetometer, which was operated between 1.8 and 300 K for dc-applied fields that range from 0 to 5 T. Microcrystalline samples were dispersed in Vaseline in order to avoid torquing of the crystallites. The sample mulls were contained in a calibrated gelatin capsule held at the center of a drinking straw that was fixed at the end of the sample rod. Alternating current (ac) susceptibilities were carried out under an oscillating ac field of 3.5 Oe with frequencies ranging from 0.1 to 1500 Hz.

Computational Details. *Ab Initio Calculations.* Using MOLCAS 7.8,[24] ab initio calculations were performed on the trivalent lanthanide ions Dy, Tb, and Ho, using the single-crystal structural data. In complexes **1**−**3**, the anisotropy of a single Ln^{III} ion was calculated on the basis of the X-ray determined geometry and by replacement of the neighboring Ln^{III} ion with a diamagnetic La^{III} ion. Relativistic effects are taken into account on the basis of the Douglas−Kroll Hamiltonian.[25] The spin-free Eigen states were achieved by the complete active space self-consistent field (CASSCF) method.[26] We have employed the [ANO-RCC...8s7p5d3f2g1h] basis set[27] for Dy, Tb, and Ho atoms, the [ANO-RCC...3s2p] basis set for C atoms, the [ANO-RCC...2s] basis set for H atoms, the [ANO-RCC...3s2p1d] basis set for N atoms, the [ANO-RCC...5s4p2d] basis set for Co, K, Zn, and Ti atoms, and the [ANO-RCC...3s2p1d] basis set for O atoms. The CASSCF calculations that were performed included 9 electrons across 7 4f orbitals of the Dy^{3+} ion, 8 electrons across 7 4f orbitals of the Tb^{3+} ion, and 10 electrons across 7 4f orbitals of the Ho^{3+} ion in **1**−**3**, respectively. With this active space, 21 roots in the configuration

DOI: 10.1021/acs.inorgchem.6b02720
Inorg. Chem. 2017, 56, 2518−2532

interaction (CI) procedure were computed for complex **1**. We also considered 7 septet excited states, 140 quintet excited states, and 195 triplet excited states for complex **2** and 35 quintet excited states, 210 triplet excited states, and 195 singlet excited states for complex **3** in the calculations to compute the anisotropy.

After computing these excited states, we mixed all roots using RASSI-SO;[28] spin−orbit coupling is considered within the space of the calculated spin-free eigenstates for **2** and **3**. Moreover, these computed SO states have been considered into the SINGLE_ANISO[29] program to compute the **g** tensors. The anisotropic **g** tensors for the Dy^{III} ion, the Tb^{III} ion, and the Ho^{III} ion have been computed with 8, 7, and 11 low-lying doublets. Cholesky decomposition for 2-electron integrals has been employed throughout our calculations. Crystal-field parameters have been extracted using the SINGLE_ANISO code, as implemented in MOLCAS 7.8. The exchange interactions have been computed between the Ln^{III} ions within each complex by fitting with the experimental data using the Lines model and employing the POLY_ANISO module.[30]

In addition to studying complexes **1**−**3**, we have modeled a dinuclear $\{Dy^{III}_2\}$ unit using the crystal structure of **1** to explore the effect the diamagnetic Co^{III} ions have on magnetization blocking of **1**. The structure of the model complex is reported as **1a**. Furthermore, we have modeled three further complexes, $\{K^{I}_2Dy^{III}_2\}$ (**1b**), $\{Zn^{II}_2Dy^{III}_2\}$ (**1c**), and $\{Ti^{IV}_2Dy^{III}_2\}$ (**1d**), using the X-ray structure of **1** by replacing the Co^{III} ions with K^{I}, Zn^{II}, and Ti^{IV} ions, respectively, to explore the effect that other cationic diamagnetic ions of varying charge have on the magnetic properties and how they compare with the tricationic diamagnetic ion (Co^{III}) in magnetization blocking.

Density Functional Theory Calculations. The exchange interaction between Ln^{III} ions has been validated using the density functional theory (DFT) method by replacing the Dy^{III} ions with Gd^{III} (**1e**) ions and keeping the positions of the other atoms the same as those determined by the X-ray structure of **1**. The DFT method has also been utilized to predict the Mulliken spin charges of the modeled structures $\{Gd^{III}_2\}$ (**1f**), $\{K^{I}_2Gd^{III}_2\}$ (**1g**), $\{Zn^{II}_2Gd^{III}_2\}$ (**1h**), and $\{Ti^{IV}_2Gd^{III}_2\}$ (**1i**). The DFT calculations combined with the broken symmetry (BS) approach[31] has been employed to compute the J value of these complexes. The BS method has a proven record of yielding good numerical estimates of J constants for a variety of complexes[32] such as dinuclear[33] and polynuclear complexes.[14c,32a,34] The DFT calculations were performed using the B3LYP functional[35] with the Gaussian 09 suite of programs.[36] We have employed the double-ζ quality basis set that employs the Cundari−Stevens (CS) relativistic effective core potential on the Gd atom[37] and Ahlrich's[38] triple-ζ-quality basis set for the rest of the atoms. The following Hamiltonian was used to estimate the exchange interaction (J) in **1c**:

$$\hat{H} = -2J(S_{Gd1}S_{Gd2}) \quad (1)$$

The computed exchange coupling constants for the Gd^{III}−Gd^{III} pair was rescaled to the spin of the Dy^{III} ion by multiplying them by the spin of Dy^{III} ($S = 5/2$) and dividing by the spin of Gd^{III} ($S = 7/2$).[12b] Similarly, the Gd^{III}−Gd^{III} pair was rescaled for the Tb ion ($S = 3$) and the Ho ion ($S = 2$). The resultant J values are in good agreement with the fitted values.

RESULTS AND DISCUSSION

Syntheses and Crystal Structures. The reaction of $Co(NO_3)_2{\cdot}6H_2O$ and $Ln(NO_3)_3{\cdot}6H_2O$ (Ln = Dy, Tb, Ho) with $mdeaH_2$ and *o*-toluic acid in acetonitrile, followed by the removal of the solvent and redissolution in MeOH/^{i}PrOH (1/1), yielded green crystals from the solution when it was layered with diethyl ether (Scheme 1). Analysis of the single-crystal X-ray data revealed a family of tetranuclear butterfly complexes of general formula $[Co^{III}_2Ln^{III}_2(\mu_3\text{-}OH)_2(o\text{-}tol)_4(mdea)_2(NO_3)_2]$ (Ln = Dy (**1**), Tb(**2**), Ho (**3**)). This family of complexes is a variation of previously reported $\{Co^{III}_2Ln^{III}_2\}$ butterfly complexes.[17,39] Two $[\mu_3\text{-}OH]^-$ bridging ligands are now present in place of $[\mu_3\text{-}OMe]^-$, a consequence of the choice of solvent used for crystallization, and *o*-toluic acid was used for the first time as the choice of carboxylic acid.

Scheme 1. Reaction Scheme Used To Isolate Tetranuclear Compounds 1−3

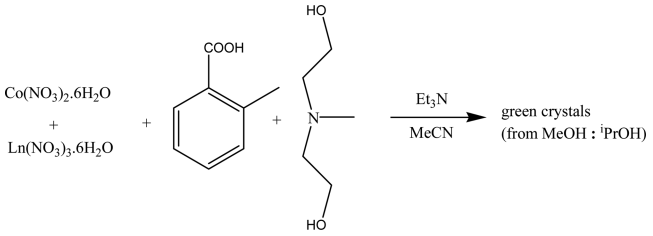

Compounds **1** and **2** are isostructural (see Table S1 in the Supporting Information for crystallographic details of **1** and **2**); however, single crystals suitable for X-ray diffraction could not be obtained for **3** and therefore the isostructural nature and purity of **3** were determined by powder X-ray diffraction (Figure S1 in the Supporting Information). A description of the Dy^{III} analogue **1** will be given here and is representative of **1**−**3**. Complex **1** (Figure 1) is a heterometallic tetranuclear complex

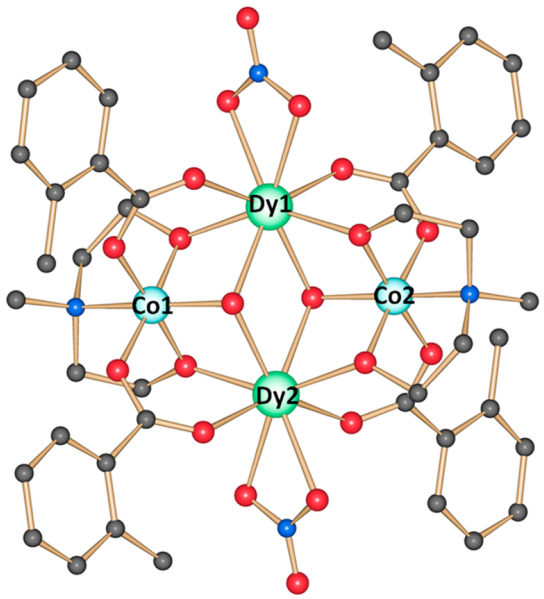

Figure 1. Molecular structure of complex **1**. The solvent and H atoms are omitted for clarity. Color scheme: Co^{III}, sky blue; Dy^{III}, green; O, red; N, blue; C, light gray. Complexes **2** and **3** are isostructural with **1**, with the Tb^{III} and Ho^{III} ions replacing the Dy^{III} sites.

that crystallizes in the triclinic space group $P\bar{1}$; the asymmetric unit contains half of the complex, which lies upon an inversion center. The metallic core consists of two Co^{III} and two Dy^{III} ions, displaying a planar "butterfly" (or diamond) motif. The Dy^{III} ions occupy the body positions and the Co^{III} ions the outer wingtips (Figure 1). The core is stabilized by two μ_3-hydroxide ligands, both bridging to two Dy^{III} ions and one Co^{III} ion. Around the periphery of the cluster, there are four *o*-toluate ligands, bridging a Co^{III} to a Dy^{III} ion. There are also two doubly deprotonated $(mdea)^{2-}$ ligands, with the N atom coordinating to an outer Co^{III} ion and with the two O atoms bridging from the Co^{III} to the body Dy^{III} ions. Both Dy^{III} ions are chelated by a $(NO_3)^-$ ligand through two O atoms. The two Co^{III} ions are six-coordinate with octahedral geometries,

DOI: 10.1021/acs.inorgchem.6b02720
Inorg. Chem. 2017, 56, 2518−2532

and the two Dy^{III} ions are eight-coordinate with distorted-square-antiprismatic geometries, as identified using the SHAPE program (see the theoretical section below).[40] The packing diagrams of **1** and **2** reveal offset aromatic $\pi-\pi$ intercluster interactions (highlighted by the dashed lines in Figure S2 in the Supporting Information).

Magnetic Properties. *Direct Current Magnetic Susceptibility Measurements.* The variation of the direct current (dc) magnetic susceptibility product $\chi_M T$ versus temperature for complexes **1**−**3** is shown in Figure 2. The room temperature

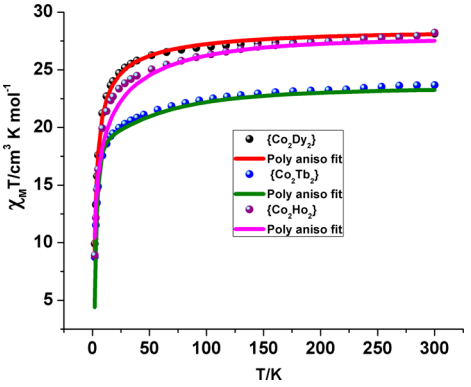

Figure 2. Plots of $\chi_M T$ versus T plots for **1**−**3** (dotted line). The solid lines are fits of the data using the Lines model employing the POLY_ANISO program.

$\chi_M T$ values of 28.14, 23.68, and 28.22 cm^3 K mol^{-1} for **1**−**3**, respectively, are in good agreement with the values expected for two Dy^{III} (S = 5/2, L = 5, $^6H_{15/2}$, g = 4/3, C = 14.17 cm^3 K mol^{-1}), two Tb^{III} (S = 3, L = 3, $^7F_6$, g = 3/2, C = 11.82 cm^3 K mol^{-1}), and two Ho^{III} (S = 2, L = 6, $^5I_8$, g = 5/4, C = 14.075 cm^3 K mol^{-1}) ions, of 28.34, 23.64. and 28.15 cm^3 K mol^{-1}, respectively. The decrease in the $\chi_M T$ product (at H_{dc} = 1 T) for **1**−**3**, from room temperature to 1.8 K, is indicative of the presence of thermal depopulation of the Ln^{III} m_J levels, combined perhaps with weak antiferromagnetic interactions between the Ln^{III} ions (see later for the analysis of the Ln^{III}−Ln^{III} magnetic exchange interaction). The isothermal magnetization M vs H plots reveal similar profiles (Figure S3 in the Supporting Information) for **1** − **3**, with a rapid increase in magnetization below 2 T, before following a more gradual linearlike increase, without saturating, thus signifying that a significant anisotropy and/or low-lying excited states are present.

Alternating Current Magnetic Susceptibility Measurements. Alternating current (ac) magnetic susceptibility experiments were performed to investigate the dynamics of relaxation of the magnetization. Measurements for compound **1** were implemented in an ac magnetic field of 3.5 Oe, oscillating at frequencies ranging from 0.1 to 1500 Hz and at temperatures between 2 and 17 K. The plot of χ_M'' versus frequency (ν) reveals temperature-dependent out-of-phase (χ_M'') susceptibility signals, confirming the presence of slow relaxation of the magnetization for **1**, and SMM behavior (Figure 3, top). Peak maxima are observed for χ_M'' between 2 and 8 K which are found to be temperature dependent over the entire frequency range. From these data, magnetization relaxation times (τ) are extracted. From the frequency-dependent behavior, it was found that the relaxation follows a thermally activated mechanism above 6 K, and the plot of ln τ vs $1/T$ is shown

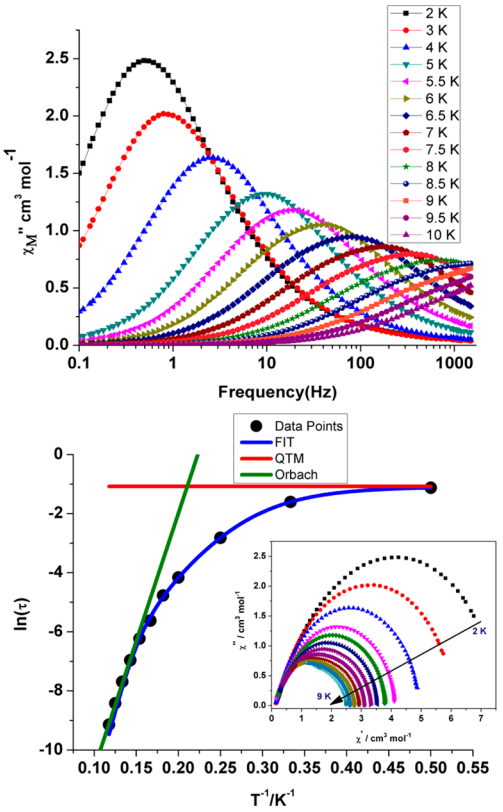

Figure 3. (top) Frequency dependence of χ_M'' for **1** in a zero applied dc field, with an ac magnetic field of 3.5 Oe. (bottom) Magnetization relaxation time (τ), plotted as ln τ versus T^{-1} for compound **1**. The solid green line corresponds to fitting of the Orbach relaxation process, and the solid blue line represents the fitting to multiple relaxation processes. The horizontal red line represents the QTM relaxation time. (bottom inset) Cole−Cole plots between 2 and 9 K.

in Figure 3, bottom. Below 5.5 K, the plot deviates from linearity, indicating that QTM and possibly other relaxation mechanisms are becoming active. It is found at 2 K that the relaxation becomes close to being independent of temperature, indicating a crossover to a pure quantum tunneling mechanism of relaxation. The magnetic relaxation data were modeled using various relaxation processes, with the following general equation employed:[10,41]

$$1/\tau = 1/\tau_{QTM} + AT + CT^n + \tau_0^{-1} \exp(U_{eff}/k_B T)$$

where the first term corresponds to the relaxation process via a quantum tunneling pathway, the second term models the direct process, the third term corresponds to relaxation via a Raman process, and the fourth term accounts for the Orbach relaxation pathway. Many fits were attempted using a number of variable parameters in the equation. The linear fit (indicated by a solid green line) corresponds exclusively to the Orbach relaxation pathway. The best fit for the Arrhenius plot could be obtained by considering the Orbach and Raman relaxation process, with the value of the Raman exponent n being closer to 6. The values obtained from the best fit are n = 6.6 (T), C = 0.00013 s^{-1} K^{-3} (T), U_{eff} = 116.9 (2) K (81.2 cm^{-1}), and τ_0 = 9.8 × 10^{-9} s (R^2 = 0.9997). This result indicates a large barrier to thermal relaxation, with a pre-exponential factor of between 10^{-6} and 10^{-11} s, which is consistent with that expected of an SMM.[2] A QTM relaxation time, τ_{QTM}, of 0.34 s is estimated. The Cole−Cole plots of χ_M' versus χ_M'' data reveal semicircular

DOI: 10.1021/acs.inorgchem.6b02720
Inorg. Chem. 2017, 56, 2518−2532

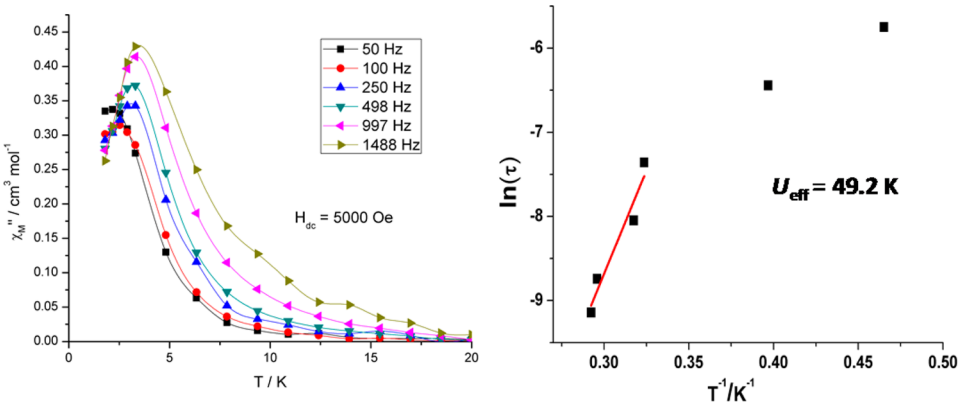

Figure 4. (left) Plot of χ_M'' versus T at the frequencies indicated for **2**, with H_{dc} = 5000 Oe. (right) Magnetization relaxation time (τ), plotted as ln τ versus T^{-1} for compound **2** from the ac data provided on the left.

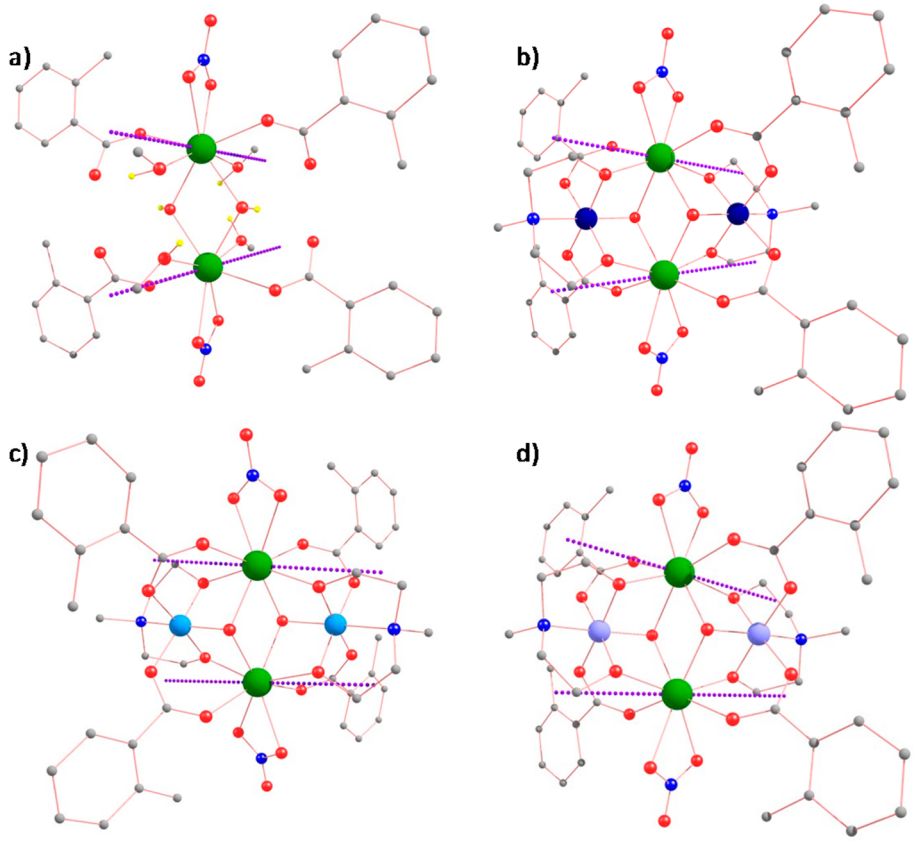

Figure 5. Modeled structures of complexes (a) **1a**, (b) **1b**, (c) **1c**, and (d) **1d**. Most of the H atoms are omitted for clarity. Color scheme: Dy^{III}, green; K^{I}, dark blue; Zn^{II}, sky blue; Ti^{IV}, pale violet; O, red; N, blue; C, light gray; H, yellow. The dotted violet lines are the g_{zz} directions of Dy^{III} ions.

profiles indicating a single relaxation process at temperatures 2−9 K (Figure 3, bottom inset).

ac magnetic measurements for the isostructural analogues **2** and **3** reveal an absence of out-of-phase susceptibility peaks in a zero static dc field but show out-of-phase (χ_M'') susceptibility signals in the presence of applied static dc fields of 5000 and 2000 Oe, respectively (Figure 4, left, and Figure S4 in the Supporting Information). The absence of SMM behavior in zero magnetic field is attributed to fast QTM. This relaxation pathway can, to some extent, be suppressed upon the application of a static dc magnetic field, which is observed for **2** and **3**, allowing for the observation of the thermally activated relaxation mechanism. Analysis of the relaxation data for **2** revealed that the plot of ln τ vs $1/T$ is linear above 3.1 K, before deviating from linearity below these temperatures—crossing over from a thermally activated process to a quantum tunneling relaxation regime (Figure 4, right). Fitting to the Arrhenius law ($\tau = \tau_0 \exp(U_{eff}/k_BT)$) afforded values of U_{eff} = 49.2 K (34.2 cm^{-1}) and $\tau_0 = 6.6 \times 10^{-11}$ s (R^2 = 0.9153).

The anisotropy barrier of **1** (81.2 cm^{-1}/116.9 K) falls within the range of that previously reported for $\{Co^{III}_2Dy^{III}_2\}$ butterfly complexes (14−170 K).[17] The loss of SMM behavior for **2** and **3** in a 0 Oe dc field is a common problem for non-Kramers ions such as Tb^{III} and Ho^{III} and is a problematic finding, as it

DOI: 10.1021/acs.inorgchem.6b02720
Inorg. Chem. 2017, 56, 2518−2532

precludes the use (in most cases) of the extremely large anisotropy both these ions possess.[42] To understand the loss of slow magnetic relaxation, we have performed ab initio calculations to probe the electronic structures of **1**−**3**. Further, we have used ab initio methods to probe the role the Co^{III} ion plays in the stabilization of the slow magnetic relaxation of **1**. After recently investigating the influence of diamagnetic 3d ions on the SMM properties of heterometallic 3d−4f complexes, we found that the diamagnetic ion has a significant influence on the electronic structure of the Ln^{III} ion(s) and thus on the magnetic relaxation behavior.[16d] In our previous $\{Co^{III}_2Ln^{III}_2\}$ work we assumed that the diamagnetic Co^{III} ions did not contribute to the slow magnetic relaxation behavior of the complex.[17] However, in the light of recent findings we have hypothetically probed the electronic structure of **1** in the absence of the two Co^{III} ions to see how these ions influence the SMM behavior. Furthermore, we have also investigated what effect replacing the tricationic diamagnetic Co^{III} ion with monocationic K^+, dicationic Zn^{II}, and tetracationic Ti^{IV} diamagnetic ions have on the SMM behavior/properties. As noted above, we have labeled these model structures as **1a** (no diamagnetic ion), **1b** (K^+ ions), **1c** (Zn^{II} ions), and **1d** (Ti^{IV} ions) (Figure 5).

Anisotropy Calculations. Ab initio calculations on complexes **1**−**3** were performed with the MOLCAS 7.8 program[24] of the CASSCF/RASSI-SO/SINGLE_ANISO type. Calculations for **1** and **2** were computed using their X-ray structures, while for complex **3**, the X-ray structure of complex **2** was utilized. In all of these calculations the neighboring Ln^{III} ion was computationally substituted by a diamagnetic La^{III} ion. Because the Co^{III} ions are diamagnetic (**1**−**3**), these were not altered in all calculations (see Computational Details). Initially, a relaxation mechanism based on the single-ion anisotropy of the lanthanide ions will be discussed, and this will be followed by the analysis of the dinuclear framework, incorporating the weak magnetic exchange coupling between the two Ln^{III} centers. At very low temperatures, the coupled systems are likely to give a realistic picture; however, at higher temperatures, where the thermal energies are much greater than the exchange coupling, one can expect the relaxation from individual Ln^{III} ions to be operational.

ac magnetic susceptibility measurements reveal SMM behavior for complex **1** and the possibility of SMM behavior for **2** and **3**. As slow magnetic relaxation behavior often originates from the anisotropy of the individual Ln^{III} ions, we have quantitatively explored the anisotropy of both Ln^{III} centers in **1**−**3** using ab initio methods. The coordination environment and geometry of each individual Ln^{III} ion were probed using the SHAPE program,[40] which revealed that the Ln^{III} ions are in a similar environment for each complex. The coordination geometry is best described by a square antiprism. Minor deviations of 2.0 for the Dy^{III} ions in **1** and 2.1 for Tb^{III} ions in **2** are observed with respect to the square antiprism. The calculated electronic and magnetic properties of both Ln^{III} ions suggest that the local **g** tensors in the ground Kramers doublet (KDs) for **1** and ground Ising doublets (**2** and **3**) are strongly axial, revealing a large g_z value (see Table 1 and Table S3 in the Supporting Information), suggesting that the single-ion anisotropy can lead to the slow magnetic relaxation in **1**−**3**. The orientations of the main anisotropy axes in the ground doublets for **1**−**3** are shown in Figure 6. It is found that the directions of the main anisotropy axes in **1** are parallel to the Co···Co vector, lying approximately in the direction of the O−Dy−O bond (methoxy O atoms of the $mdea^{2-}$ ligands), tilted by 24.1° from the O−Dy−O bond vector. However, in complexes **2** and **3**, the g_{zz} axes are found to deviate significantly from the Co···Co vector and lie in the direction of the $O_{o\text{-tol}}$−Tb^{III} and $O_{o\text{-tol}}$−Ho^{III} bonds. For complex **3** the orientations of the anisotropy axes of each individual Ho^{III} ion are found to be different, and this is reflected in the computed *g* anisotropy.

Table 1. Low-Lying Energies (cm^{-1}) and g Tensors of the Ln^{III} Fragments That Originate from the Corresponding Ground Atomic Multiplet in 1−3

energy					
1		**2**		**3**	
Dy1	Dy2	Tb1	Tb2	Ho1	Ho2
0.000	0.000	0.000	0.000	0.000	0.000
77.518	77.944	0.180	0.180	4.496	2.803
187.362	188.428	138.003	138.003	30.500	21.383
245.927	247.047	143.825	143.825	47.445	35.528
273.979	275.357	224.498	224.498	66.331	81.147
350.793	351.836	275.607	275.607	97.271	112.692
414.201	415.025	301.178	301.178	109.880	128.906
675.248	675.816	430.456	430.456	155.589	181.827
		432.902	432.902	161.296	189.002
		586.366	586.366	194.535	209.606
		586.853	586.853	210.938	220.977

g tensor						
	ground Kramers doublet (**1**)		ground Ising doublet (**2**)		ground Ising doublet (**3**)	
	Dy1	Dy2	Tb1	Tb2	Ho1	Ho2
g_x	0.0005	0.0004	0.0000	0.0000	0.0000	0.0000
g_y	0.0043	0.0043	0.0000	0.0000	0.0000	0.0000
g_z	19.9331	19.9282	17.2555	17.2515	16.1007	16.6344

The computed energy gap between the ground KDs or the Ising doublets and the excited states are shown in Table 1 and Table S2 in the Supporting Information. The presence of small QTM (0.8×10^{-3} μ_B) at the ground state for both Dy^{III} ions in **1** causes magnetic relaxation to occur via excited KDs. At the first excited state, however, thermally activated QTM/Orbach processes are operative and thus the magnetization relaxes back to the ground state from the first excited state. The average of the computed energies of the first excited Kramers doublet for the two Dy^{III} ions in **1** correlate to an energy barrier (U_{eff}) of 77.7 cm^{-1}. This is in good agreement with the experimentally determined barrier (81.2 cm^{-1}), although the experimental value is slightly greater than calculated which is probably due to the exclusion of intermolecular and hyperfine interactions in the calculation and the possibility of a non-Orbach relaxation mechanism. A qualitative mechanism for the magnetic relaxation for the two Dy^{III} sites in **1** obtained from the ab initio calculations is shown in Figure 7. For complexes **2** and **3**, however, we discover from the calculations that the tunneling gap between the ground-state single-ion Tb^{III} and Ho^{III} sites are very large: ∼0.18 cm^{-1} (for **2**) and 2.8−4.5 cm^{-1} (for **3**) (see Table 1). This supports the experimental absence of SMM behavior from the ac measurements in zero dc field for **2** and **3**. The application of a dc field can lift the degeneracy of the Ising doublets and quench QTM to a certain extent. This is found to be the case from the experiments. As the tunnel splitting parameter in complex **3** (2.8−4.5 cm^{-1}) is one order of

DOI: 10.1021/acs.inorgchem.6b02720
Inorg. Chem. 2017, 56, 2518−2532

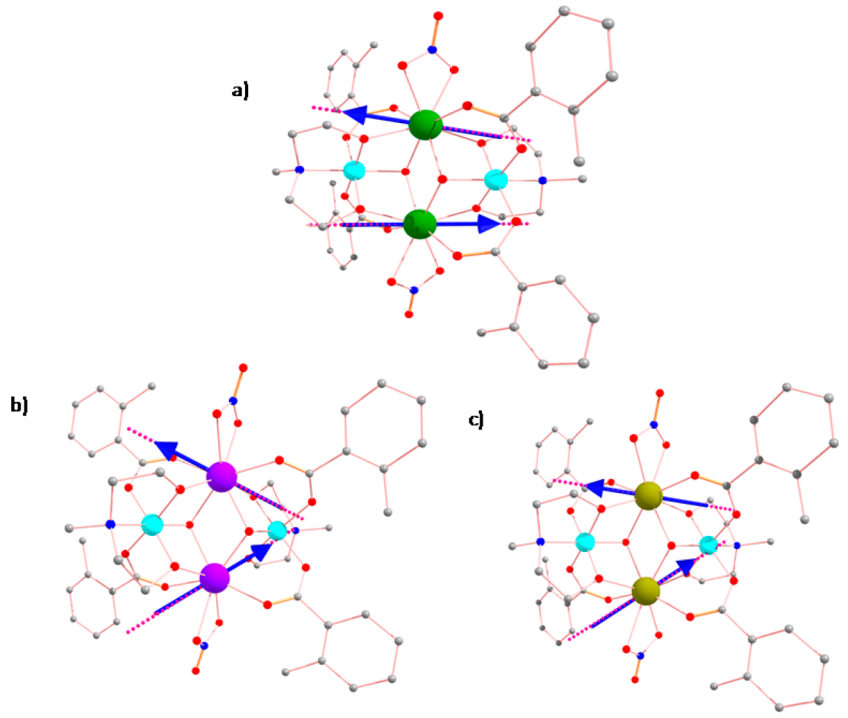

Figure 6. Orientations of the local magnetic moments in the ground doublet of complexes (a) **1**, (b) **2**, and (c) **3**. Blue arrows show the antiferromagnetic coupling of the local magnetic moments of the Ln^{III} ions in the ground state (vide infra).

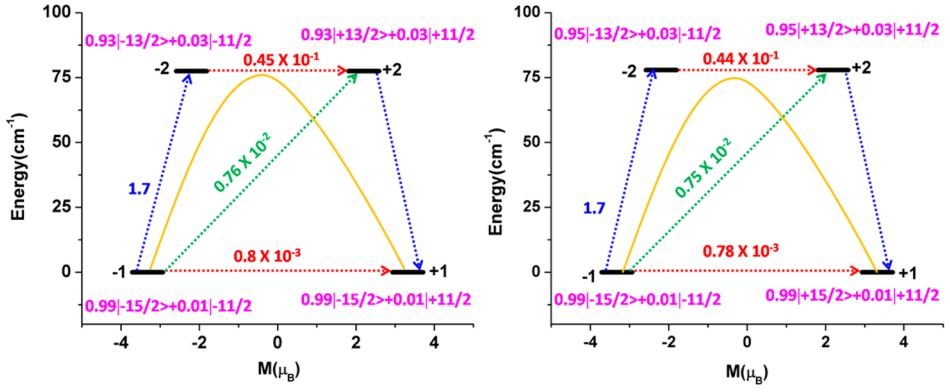

Figure 7. Magnetization blocking barrier for (left) the Dy1 site (right) and the Dy2 site in **1** computed ab initio. The thick black line indicates the Kramers doublets (KDs) as a function of computed magnetic moment. The green/blue arrows show the possible pathway through Orbach/Raman relaxation. The dotted red lines represent the presence of QTM/TA-QTM between the connecting pairs. The numbers provided at each arrow are the mean absolute values for the corresponding matrix element of the transition magnetic moment. The yellow curve indicates the most possible relaxation pathway.

magnitude larger than that estimated for complex **2** (0.18 cm^{-1}), it fits nicely with the experimental observation that complex **2** exhibits maxima in the out-of-phase signal when a moderate dc field is applied, whereas complex **3** does not.

The ground state Kramers doublet of the Dy^{III} ions are estimated to be pure $m_J = \pm 15/2$ ($g_z \approx 20$). The Tb^{III} ion ground doublet is $m_J = \pm 6$ ($g_z \approx 18.0$), and the Ho^{III} ground state resembles that of a $m_J = \pm 7$ state, as the computed anisotropy is close to $g_z \approx 17.5$ but far from the pure $m_J = \pm 8$ state of $g_z \approx 20$. The computed Mulliken charges for complex **1** are shown in Figure 8a. Among all the coordinated atoms, the largest charges are noticed on the μ_2- and μ_3-alkoxo oxygen atoms connected to the Co^{III} ion. As the Dy^{III} ion electron density has an oblate shape, the β-electron density will lie perpendicular to the direction of maximum electrostatic repulsion, while the g_{zz} axis lies along the atoms possessing the "largest" charges. This rationalizes the observation of the parallel g_{zz} orientation observed in complex **1**. The "larger" charges found on the alkoxo oxygen atoms, in comparison to other ligand O atoms, are due to their vicinity of the diamagnetic Co^{III} ion, which polarizes the oxygen atoms. The charge of the ligand donor atoms also influence the crystal field splitting, with the first excited state found to be 77.5 cm^{-1} higher in energy.

As the electrostatic interactions are the same for the Tb^{III} and Ho^{III} complexes, in comparison to **1**, one can expect a similar picture. However, Tb^{III} is relatively more oblate than Dy^{III}, while Ho^{III} is less oblate in comparison to Dy^{III}.[3a,43] This means that the electrostatic repulsion of the strongly negative oxygen atoms connected to the Co^{III} ion will have the strongest influence on the electronic structure of the Tb^{III} ions, followed by Dy^{III}, and have the weakest influence on the Ho^{III} ions. This

DOI: 10.1021/acs.inorgchem.6b02720
Inorg. Chem. 2017, 56, 2518−2532

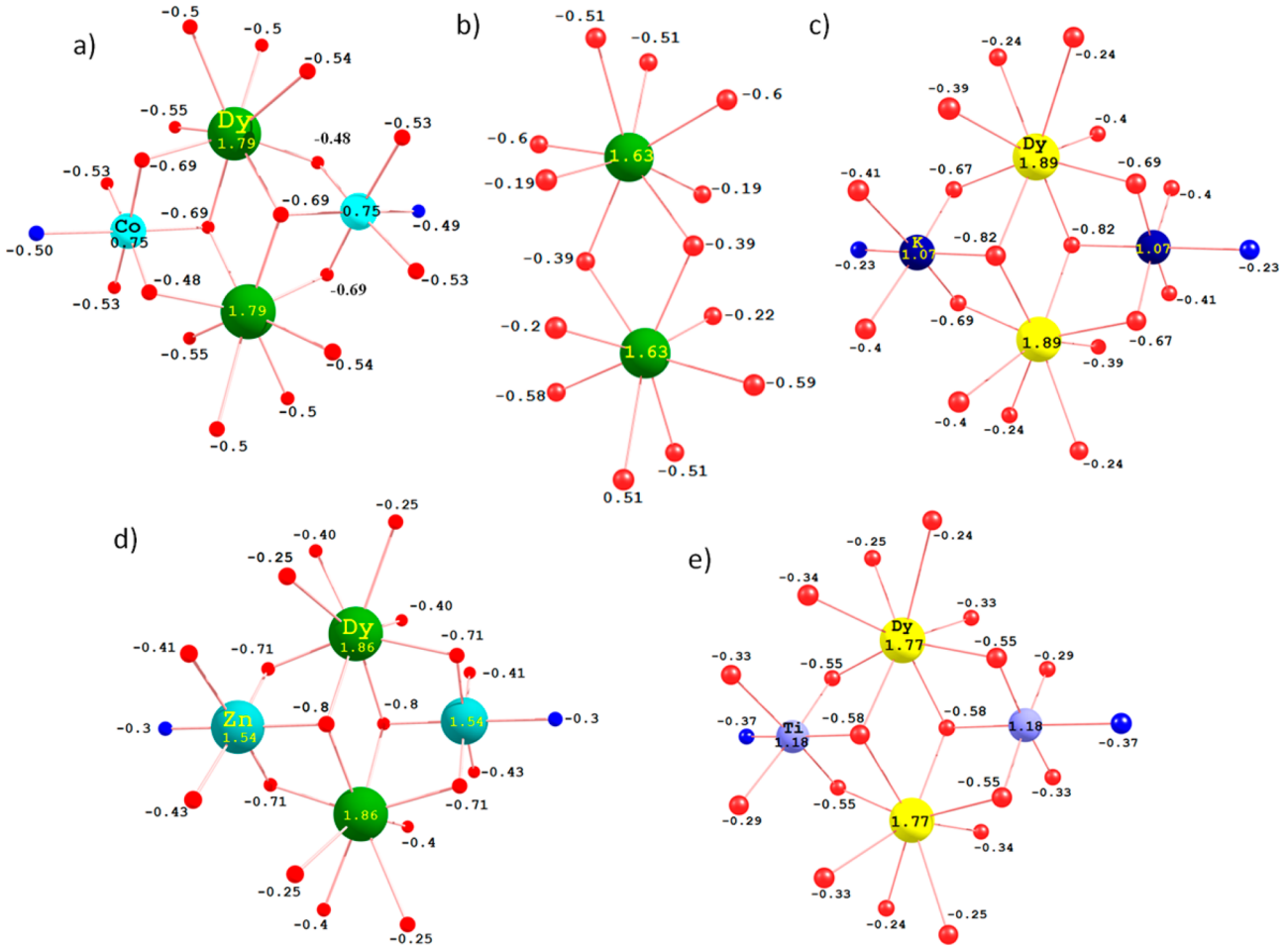

Figure 8. DFT-computed Mulliken charges on the donor atoms of complexes (a) **1**, (b) **1a**, (c) **1b**, (d) **1c**, and (e) **1d**.

is clearly reflected in the ground-state−first-excited-state energy gaps, where the single-ion Tb^{III} energy gap is calculated to be 138.0 cm^{-1}, whereas the Dy^{III} energy gap is approximately half of this value at 77.5 cm^{-1}, with the Ho^{III} single-ion energy splitting being the smallest at 30 cm^{-1}. On the basis of this evidence, one can expect SMM behavior with longer relaxation times (at a fixed temperature) to be observed for the Tb^{III} complex, followed by the Dy^{III} complex, and the Ho^{III} complex would have the fastest relaxation time if a thermally activated process were favored. However, the magnetic relaxation in lanthanide-based complexes is dominated by QTM relaxation pathways and, as Tb^{III} and Ho^{III} are non-Kramers ions, the tunneling, as indicated above, plays a prominent role in quenching the magnetization blockade.

To understand the role of the magnetic exchange interaction between the 4f ions in governing the magnetization relaxation, we have analyzed the magnetic exchange using the POLY_ANISO routine.[30] The exchange interactions were calculated within the Lines model,[44] which describes the exchange coupling between the spin moments of magnetic sites in **1**−**3**. The calculations reproduce the susceptibility and magnetization measurements well; fits of the magnetic data are shown in Figure 2. The exchange parameters obtained are summarized in Table 2. It was found that the Ln^{III}−Ln^{III} exchange interactions for **1**−**3** are antiferromagnetic. To validate the exchange coupling constants of the Ln^{III}−Ln^{III} pairs, we have performed DFT calculations for the Gd^{III}−Gd^{III} pair (see Computational Details). The calculations yielded antiferromagnetic exchange interactions between the Gd^{III} centers, with the J value estimated to be −0.04 cm^{-1}, which is in good agreement with the value obtained from the Lines model.

Table 2. Magnetic Exchange Interactions (cm^{-1}) between Magnetic Lanthanide Ions in 1−3

	magnetic interaction (Ln^{III}−Ln^{III})	
	calcd J_{exch}(DFT)	Lines J_{exch}
1	−0.029	−0.05
2	−0.034	−0.042
3	−0.023	−0.012

The anisotropy barriers were then computed with the lowest energy states of each Ln^{III} ion, which were coupled using the POLY_ANISO routine. The energies, the corresponding tunneling gaps, and the g_Z values of the lowest exchange-coupled states of complexes **1**−**3** are given in Tables S5 and S6 in the Supporting Information. It is found that the computed barrier energies of each complex correlate nicely with the experimentally determined barriers. For complex **1**, although weak exchange introduces several low-lying states, the relaxation is found to occur via excited states lying 78.2 cm^{-1} above the ground state, due to the tunneling of the magnetization. The coupled state anisotropy barrier, U_{cal} = 78.2 cm^{-1}, therefore agrees quite well with the experimentally determined value of 81.2 cm^{-1} (see Figure 9a).

For complex **2**, on the other hand, the magnetic exchange interaction is not strong enough to quench the quantum

DOI: 10.1021/acs.inorgchem.6b02720
Inorg. Chem. 2017, 56, 2518−2532

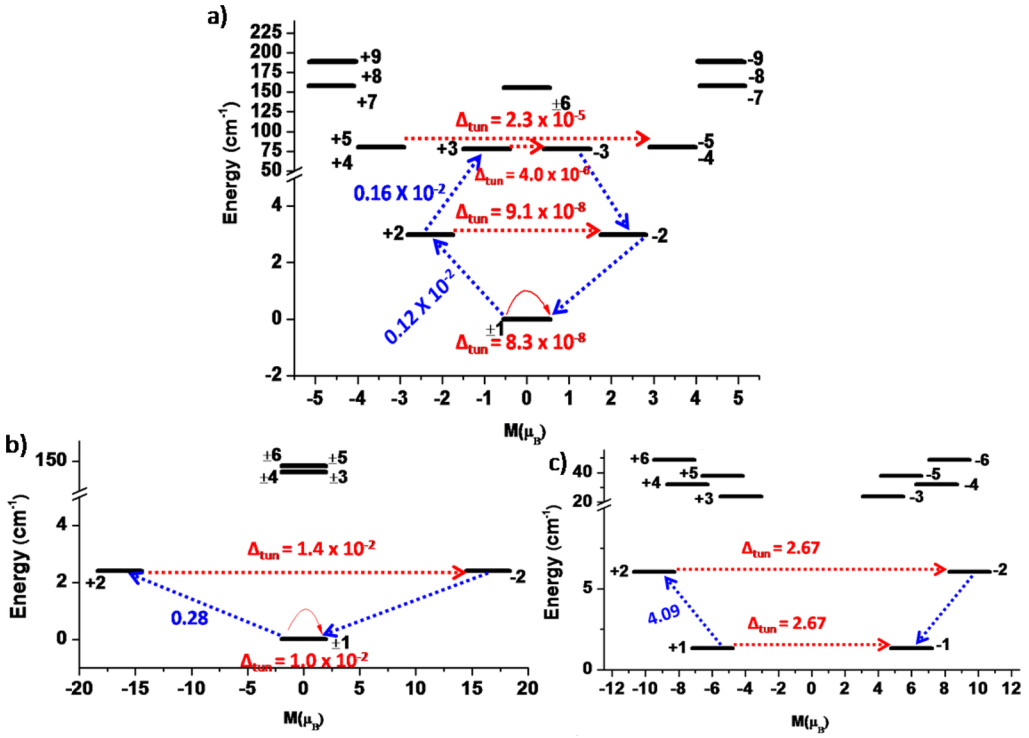

Figure 9. Low-lying exchange spectra in (a) **1**, (b) **2**, and (c) **3**. The exchange states are placed on the diagram according to their magnetic moments (bold black lines). The red arrows show the tunneling transitions (energy splitting) within each doublet state, while the green/blue arrows show the possible pathway through Orbach/Raman relaxation. The numbers at the paths are averaged transition moments in μ_B, connecting the corresponding states.

Table 3. Low-Lying Energies (cm^{-1}) and g Tensors of Dy^{III} Fragments That Originate from the Corresponding Ground Atomic Multiplet in Model Complexes 1a–d

energy							
1a		**1b**		**1c**		**1d**	
Dy1	Dy2	Dy1	Dy2	Dy1	Dy2	Dy1	Dy2
0.0	0.0	0.000	0.000	0.0	0.0	0.000	0.000
88.5	71.6	167.561	168.031	127.2	127.7	47.867	48.499
172.1	132.5	358.937	359.799	288.8	289.6	93.721	94.910
290.8	244.6	455.989	457.620	361.5	363.0	151.855	153.030
445.1	393.0	477.791	479.121	383.3	384.7	171.766	173.200
573.8	529.6	557.047	558.513	465.0	466.3	236.155	237.330
683.7	649.4	612.223	613.395	523.6	524.7	296.710	297.537
1005.2	1007.5	843.870	844.693	780.3	781.1	534.148	534.761
tensor							
	ground Kramers doublet (**1a**)		ground Kramers doublet (**1b**)		ground Kramers doublet (**1c**)		ground Kramers doublet (**1d**)	
	Dy1	Dy2	Dy1	Dy2	Dy1	Dy2	Dy1	Dy2
g_x	0.2219	0.3703	0.0002	0.0002	0.0011	0.0010	0.0085	0.0082
g_y	0.5212	1.0312	0.0003	0.0003	0.0015	0.0015	0.0216	0.0210
g_z	19.4198	19.0995	19.9797	19.9124	19.9747	19.9385	19.8339	19.8718

tunneling at the ground state, due to the significantly large tunnel splitting still present (1.0×10^{-2} cm^{-1}, but smaller than the single ion splitting of 0.18 cm^{-1}). This is significantly larger than that seen in **1** (8.3×10^{-8} cm^{-1}). However, the application of a large dc field (5000 Oe) will result in a Zeeman splitting greater than the tunnel splitting, leading to quenching of the tunneling, at both the ground-state and first-excited-state levels, to a certain extent. This will result in relaxation occurring via excited states, up to 138.9 cm^{-1} above the ground state (see Figure 9b). At the third excited state the tunneling splitting (6.9 $\times 10^{-2}$ cm^{-1}) is very large; therefore, the magnetization blockade is unlikely to go higher. The U_{cal} estimate of 138.9 cm^{-1} is, however, much larger than the experimentally determined value of 34.2 cm^{-1}. This discrepancy is due to the fact that complete quenching of the tunneling at the ground and first excited states is unlikely and other non-Orbach mechanisms are also operational in reducing the barrier height.

For complex **3**, on the other hand, the ground-state tunnel splitting is still exceptionally high (2.67 cm^{-1}), in comparison to the single-ion relaxation mechanism (2.8–4.5 cm^{-1}; see

DOI: 10.1021/acs.inorgchem.6b02720
Inorg. Chem. 2017, 56, 2518–2532

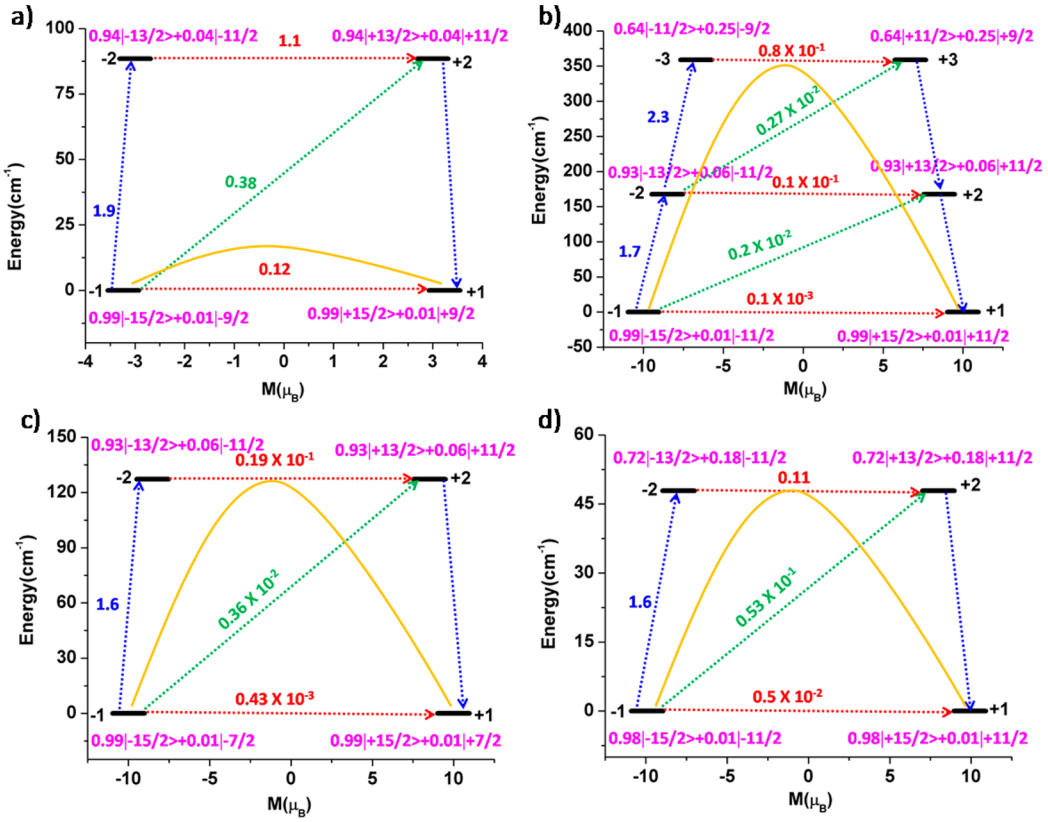

Figure 10. Magnetization blocking barrier for the Dy1 site in (a) **1a**, (b) **1b**, (c) **1c**, and (d) **1d**. The thick black line indicates the Kramers doublets (KDs) as a function of computed magnetic moment. The green/blue arrows show the possible pathway through Orbach/Raman relaxation. The dotted red lines represent the presence of QTM/TA-QTM between the connecting pairs. The numbers provided at each arrow are the mean absolute values for the corresponding matrix element of the transition magnetic moment. The yellow curve indicates the most possible relaxation pathway.

Figure 9c). This is a consequence of the weak $Ho^{III}\cdots Ho^{III}$ magnetic exchange, which displays the smallest J parameter (Table 2) of the three complexes and is therefore not strong enough to quench the tunneling of the magnetization. A tunnel splitting of 2.67 cm^{-1} in the ground state suggests that application of a dc field is unlikely to diminish the quantum tunneling relaxation pathway to observe magnetization blockade, concordant with experiments.

Role of Diamagnetic Substitution in the Mechanism of Magnetization Relaxation. A large anisotropy barrier (U_{eff}) is found to be present for **1**, and its magnitude falls within the range of that previously reported for $\{Co^{III}_2Dy^{III}_2\}$ SMMs of similar type.[17] We have shown from the above computational analysis that the electronic structure of the two Dy^{III} single ions reveal the **g** tensors in the ground Kramers doublet are strongly axial with a large g_z value and vanishingly small transverse components (g_x (0.0005), g_y (0.0043)). The SMM behavior is therefore a consequence of this electronic structure. We have therefore probed how the diamagnetic Co^{III} ion influences the electronic and magnetic behavior and what its influence is on the U_{eff} value.

To understand the role of the Co^{III} ions, we have created a model where, fictitiously, the Co^{III} ions are removed (complex **1a**; see Figure 5). Calculations reveal that the local **g** tensors of the Dy^{III} ions in the ground Kramers doublet are axial in nature; however, they now display large transverse components (g_x = 0.222, g_y = 0.521, and g_z = 19.419 for Dy1 and g_x = 0.370, g_y = 1.031, and g_z = 19.099 for Dy2). The computed energies of the first excited Kramers doublet are found to be 88.5 cm^{-1} for Dy1 and 71.6 cm^{-1} for Dy2 (see Table 3). A qualitative mechanism for magnetic relaxation at the individual Dy^{III} sites in **1a**, obtained from the ab initio calculations, is shown in Figure 10a (Dy1) and Figure S4a in the Supporting Information (Dy2). It can be seen that the tunneling probability in the ground state is now significantly higher for **1a** than for **1** (0.16 vs 0.8 × 10^{-3}, respectively, averaged over the two sites). This is essentially due to the presence of large transverse terms in the ground state. To understand the nature of the coupled state, we have assumed the $Dy^{III}\cdots Dy^{III}$ exchange for **1a** to be the same as that for complex **1**. The simulated energy levels using the POLY_ANISO routine reveal that the weak $Dy^{III}\cdots Dy^{III}$ exchange is not strong enough to quench the QTM at the ground state and thus **1a** is unlikely to exhibit SMM characteristics. This is supported by various experimental accounts, such as a similar dihydroxide bridged eight-coordinate $\{Dy^{III}_2\}$ complex which revealed an absence of SMM behavior.[45]

As the absence of the trivalent diamagnetic ion suggests the absence of SMM behavior in these complexes, thus highlighting the importance of the diamagnetic ion, we have probed how changing the diamagnetic species might affect the anisotropy barrier and thus the SMM properties. For this study we have replaced the tricationic diamagnetic ion in **1**, with monocationic, dicationic, and tetracationic diamagnetic ions. We have selected K^+, Zn^{II}, and Ti^{IV} as the ions and modeled the Co^{III} ions in complex **1** as K^+ (model **1b**), Zn^{II} (model **1c**), and Ti^{IV} (model **1d**), respectively. The calculations performed for **1b** (see Computational Details) on both Dy^{III} ions suggest that the

DOI: 10.1021/acs.inorgchem.6b02720
Inorg. Chem. 2017, 56, 2518−2532

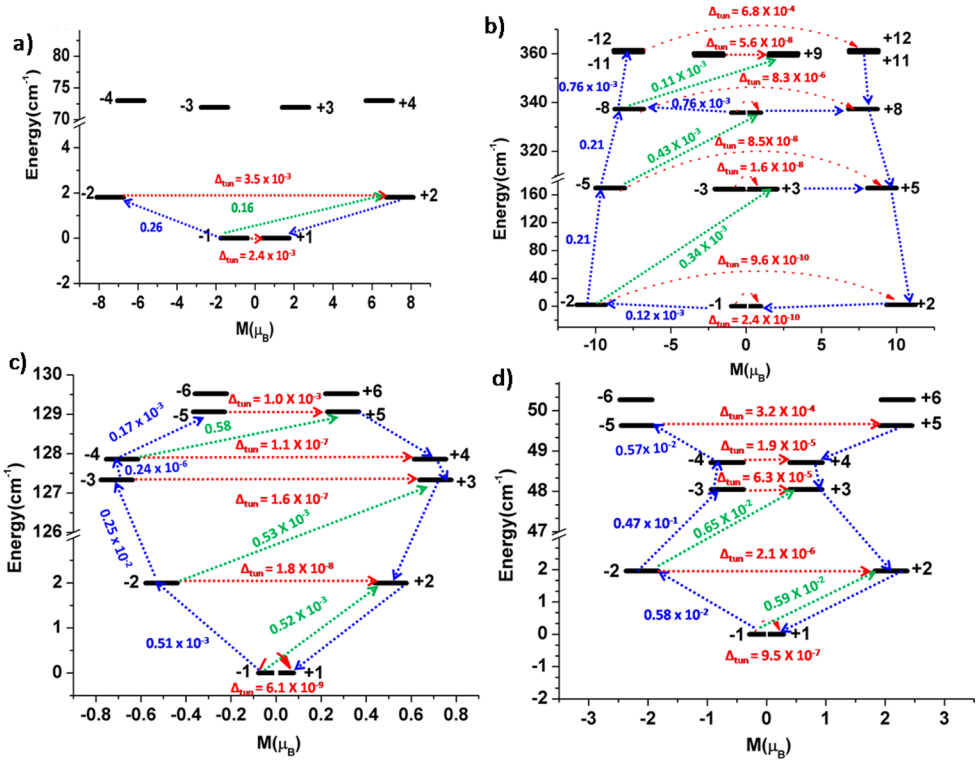

Figure 11. Low-lying exchange spectra in (a) **1a**, (b) **1b**, (c) **1c**, and (b) **1d**. The exchange states are placed on the diagram according to their magnetic moments (bold black lines). The red arrows show the tunneling transitions (energy splitting) within each doublet state, while the green/blue arrows show the possible pathway through Orbach/Raman relaxation. The numbers at the paths are averaged transition moments in μ_B, connecting the corresponding states.

local **g** tensors in the ground Kramers doublet are purely axial in nature, with very small transverse components (g_x = 0.0002, g_y = 0.0003, and g_z = 19.9797 for Dy1 and g_x = 0.0002, g_y = 0.0003, and g_z = 19.9124 for Dy2). The presence of a monocationic diamagnetic cation yields very small transverse terms similar to those for **1**, which is in contrast with model complex **1a** (no diamagnetic ion), which has a large transverse component. Due to small TA-QTM in the first excited state (tunnel probability 0.1×10^{-1} μ_B) the magnetization relaxes via the second excited state (tunnel probability 0.8×10^{-1} μ_B) and the computed energies of the Dy^{III} single-ion second excited Kramers doublet for **1b** are found to be 358.9 cm^{-1} for Dy1 and 359.8 cm^{-1} for Dy2 (see Table 3). This is larger than that observed for complex **1**, suggesting a stronger electrostatic repulsion offered by the closed-shell K^+ ion. A qualitative mechanism for the magnetic relaxation for the Dy^{III} sites in **1b** obtained from the ab initio calculations is shown in Figure 10b (Dy1) and Figure S4b in the Supporting Information (Dy2). If we assume the $Dy^{III}\cdots Dy^{III}$ exchange for **1b** to be of magnitude similar to that in **1**, we can construct an exchange coupled relaxation mechanism (see Figure 11b and Table S8 in the Supporting Information), where a smaller tunneling probability is found in the ground state (2.4×10^{-10} cm^{-1}), in comparison to the single-ion analysis. Moreover, it is found that the tunneling probability is very small (9.6×10^{-10} to 6.7×10^{-7} cm^{-1}) until the 10th excited state. Therefore, the relaxation pathway proceeds to the 11th excited state. The effect of the Dy^{III}–Dy^{III} exchange is found to suppress the tunneling for **1b**, in comparison to the single ion, leading to a barrier height of 361.4 cm^{-1}. This estimate of U_{cal} is larger than that estimated for complex **1**, which suggests the superiority of employing a monocationic diamagnetic K^+ ion in place of Co^{III}. Although the K^+model is fictitious, incorporation of K^+ in Dy^{III} cluster aggregation found to enhance the barrier height in a $\{Dy_5\}$ cluster[7a,f] supporting the above analysis.

Similarly, the calculations performed for **1c,d** (see Computational Details) on both Dy^{III} ions suggest that the local **g** tensors in the ground Kramers doublet are axial in nature, with very small transverse components (see Table 3). Three structurally analogous $\{Zn^{II}_2Dy^{III}_2\}$ complexes (see Figure S5 in the Supporting Information for details), possessing eight-coordinate Dy^{III} ions, have been reported in the literature, which offers confidence in our computed model **1c**.[46] The computed energies of the Dy^{III} single-ion first excited Kramers doublet for **1c** are found to be 127.2 cm^{-1} for Dy1 and 127.7 cm^{-1} for Dy2 (see Table 3). These values are larger than those observed for complex **1**, but smaller in comparison to **1b**, suggesting that a stronger electrostatic repulsion is also offered by the closed-shell Zn^{II} ion in comparison to that when the Co^{III} ion is present. A qualitative mechanism for the magnetic relaxation for the Dy^{III} sites in **1c** obtained from the ab initio calculations is shown in Figure 10c (Dy1) and Figure S4c in the Supporting Information (Dy2). Clearly, at the single-ion level the QTM effects on the ground-state KD (tunnel probability 0.43×10^{-3} μ_B) are quenched, leading to relaxation via the first excited state, lying at 127 cm^{-1} above the ground state. For **1c**, we also assumed the $Dy^{III}\cdots Dy^{III}$ exchange for **1c** to be of magnitude similar to that in **1** and constructed an exchange coupled relaxation mechanism (see Figure 11c and Table S9 in the Supporting Information), where a smaller tunneling probability is found in the ground state (6.1×10^{-9} cm^{-1}), in comparison to the single-ion analysis of **1c**. Moreover, it is found that the tunneling probability is also small (1.8×10^{-8} to 1.1×10^{-7} cm^{-1}) for the first three excited states. Therefore,

DOI: 10.1021/acs.inorgchem.6b02720
Inorg. Chem. 2017, 56, 2518−2532

the relaxation pathway proceeds to the fourth excited state. The effect of the Dy^{III}–Dy^{III} exchange is found to suppress the tunneling for **1c**, in comparison to the single ion, leading to a barrier height of 129.1 cm^{-1}. These calculations are supported/validated from the experimental observations of the three structurally analogous $\{Zn^{II}_2Dy^{II}_2\}$ complexes mentioned above, each of which are reported to exhibit SMM characteristics.[46] In model **1d**, the computed energies of the Dy^{III} single-ion first excited Kramers doublet is found to be 47.9 cm^{-1} for Dy1 and 48.4 cm^{-1} for Dy2 (see Table 3, Figure 10d (Dy1), and Figure S4d (Dy2)) which are smaller in comparison to those for **1** and **1b**,**c**. The exchange coupled relaxation mechanism (see Figure 11d and Table S10 in the Supporting Information) suggests that the tunneling probability is again very small from the ground state (9.5×10^{-7} to 1.9×10^{-5} cm^{-1}) up to the fourth excited state. Thus, the relaxation proceeds via the fourth excited state, leading to a barrier height of 49.6 cm^{-1}. Out of the four diamagnetic ion containing complexes studied, the most highly charged cation, the Ti^{4+} ion, displays the smallest anisotropy barrier.

We have also computed the crystal field (CF) parameters for complexes **1**–**3** and the corresponding models (**1a**–**1d**) to achieve a deeper insight into the mechanism of magnetic relaxation. The corresponding crystal field Hamiltonian is given by eq 2:

$$\hat{H}_{CF} = \sum \sum_{k=-q}^{q} B_k^q \tilde{O}_k^q \tag{2}$$

Considering that hyperfine interactions and intermolecular interactions are small or negligible, the probability of QTM between the ground state KDs is described by the CF parameters. The corresponding crystal field Hamiltonian is given as eq 2, where B_k^q is the crystal field parameter, while O_k^q is the Stevens operator. The QTM effects are dominant in a system where the nonaxial B_k^q (in which $q \neq 0$ and $k = 2, 4, 6$) terms are larger than the axial terms (in which $q = 0$ and $k = 2, 4, 6$). The computed CF parameters for complexes **1**–**3** are given in Tables S11 and S13 in the Supporting Information. For all three complexes **1**–**3**, the nonaxial terms are larger than the axial terms, reflecting the computed transverse anisotropy for the ground state. The negative sign of the computed B_2^0 parameter reveals the axial character of the ligand field, which is determined to be −4.1 (Tb^{III}), −2.4 (Dy^{III}), and −0.56 (Ho^{III}) for **2**, **1**, and **3**, respectively. The magnitude of the parameter decreases in the same order as the decrease in oblate character.[3a,43] In all cases, significant nonaxial terms are detected, suggesting prominent QTM effects. If the Co^{III} ions are removed from complex **1** (model **1a**), the nonaxial terms are enhanced significantly in comparison to **1**, leading to a larger transverse anisotropy term and fast QTM relaxation. On the other hand, if new diamagnetic ions such as K^+, Zn^{II}, and Ti^{IV} are placed in the position of the Co^{III} ion (models **1b**–**d**), the crystal field parameters are very similar to those of complex **1**, reflecting how the ground-state transverse anisotropy is affected by the presence of the diamagnetic ion in the coordination sphere. A larger barrier, in comparison to **1**, is calculated in the case of models **1b**,**c** due to the greater ground-state–excited-state gap, as the K^+ and Zn^{II} ions are found to promote a stronger electrostatic interaction (see Figure 10). This is also reflected in the computed Mulliken charges, where the K^+ and Zn^{II} ions are found to possess charges of 1.07 and 1.54, respectively, while the Co^{III} ion has a charge of 0.75. For the Co^{III} ion the reduction of the computed charge is very large in comparison to the expected formal value of 3.0, while for K^+ it is slightly more than the expected value and for Zn^{II} ions only a moderate deviation from 2.0 is noted. This is likely due to the fact that the empty e_g orbitals of the Co^{III} ion can accept electrons from the coordinating atoms, leading to a reduction of the formal charge, while this is not possible for the K^I and Zn^{II} ions. In summary, the ab initio analysis reveals barrier heights for magnetization reversal are found to be in the order (**1b**, 361.4 cm^{-1}) > (**1c**, 129.1 cm^{-1}) > (**1**, 78.2 cm^{-1}) > (**1d**, 49.6 cm^{-1}) for the diamagnetic ion series. This trend clearly suggests that, when the oxidation state of the diamagnetic ion decreases, the electronic repulsion to the bridging atoms increases, thus increasing the anisotropy barrier as well as quenching the QTM to a certain extent. The barrier heights are therefore found to correlate to the computed Mulliken charges of the μ_3-OH^- bridges, which carry a larger negative charge next to the cations of smaller charge (see Figure 8 and Tables S14–S18 and Figures S7–S9 in the Supporting Information). Attempts to isolate compounds similar to those of the model complexes **1b**–**d** studied here are currently under way in our laboratory.

CONCLUSIONS

The synthesis, magnetic, and theoretical studies of three tetranuclear $\{Co^{III}_2Ln^{III}_2\}$ butterfly complexes were carried out. ac susceptibility measurements revealed the presence of magnetic blocking for **1**, which indicates SMM behavior. An anisotropy barrier U_{eff} of 81.2 cm^{-1} was determined, with a pure quantum tunneling relaxation time, τ_{QTM}, of ∼0.34 s, which suggests that the QTM is fast. The SMM behavior is lost in the absence of a dc field for the Tb^{III} and Ho^{III} analogues; however, it can be observed in the presence of a bias direct current field. For **2** an anisotropy barrier U_{eff} of 34.2 cm^{-1} was determined. These experimental observations were rationalized via *ab initio* calculations. The influence of the diamagnetic Co^{III} ion on the relaxation behavior was also probed via ab initio and DFT calculations. The evidence strongly suggests that the Co^{III} is integral to the observation of SMM behavior in these systems and removal of Co^{III} ion found to increase the transverse anisotropy of the ground state, leading to a significant QTM relaxation process. Our calculations also predict that other diamagnetic metal ions such as K^+ and Zn^{II}, in the place of diamagnetic Co^{III}, may yield better-performing SMMs, with longer relaxation times, as their electrostatic charge polarizations are found to be larger than that computed for Co^{III} ions.

ASSOCIATED CONTENT

Supporting Information

The Supporting Information is available free of charge on the ACS Publications website at DOI: 10.1021/acs.inorgchem.6b02720.

(PDF)
(CIF)
(CIF)

AUTHOR INFORMATION

Corresponding Authors

*E-mail for K.S.M.: keith.murray@monash.edu.
*E-mail for G.R.: rajaraman@chem.iitb.ac.in.

DOI: 10.1021/acs.inorgchem.6b02720
Inorg. Chem. 2017, 56, 2518–2532

ORCID
Gopalan Rajaraman: 0000-0001-6133-3026

Notes

The authors declare no competing financial interest.

■ ACKNOWLEDGMENTS

K.S.M. thanks the Australian Research Council (ARC), and G.R. thanks the DST-SERB (EMR/2014/00024) for funding. Grants to K.S.M. and G.R. from the Australia-India AISRF fund are gratefully acknowledged. K.R.V. is thankful to the IITB-Monash Research Academy for a Ph.D. studentship. The authors thank Dr. Boujemaa Moubaraki for help with magnetism. Structural aspects of this research were undertaken on the MX1 beamline at the Australian Synchrotron, Clayton, Victoria, Australia.

■ REFERENCES

(1) (a) Christou, G.; Gatteschi, D.; Hendrickson, D. N.; Sessoli, R. Single-molecule magnets. *MRS Bull.* **2000**, *25*, 66−71. (b) Sessoli, R.; Gatteschi, D.; Caneschi, A.; Novak, M. A. Magnetic Bistability in a Metal-Ion Cluster. *Nature* **1993**, *365*, 141−143. (c) Sessoli, R.; Tsai, H. L.; Schake, A. R.; Wang, S.; Vincent, J. B.; Folting, K.; Gatteschi, D.; Christou, G.; Hendrickson, D. N. High-spin molecules: $[Mn_{12}O_{12}(O_2CR)_{16}(H_2O)_4]$. *J. Am. Chem. Soc.* **1993**, *115*, 1804−1816.

(2) Sessoli, R.; Powell, A. K. Strategies towards single molecule magnets based on lanthanide ions. *Coord. Chem. Rev.* **2009**, *253*, 2328−2341.

(3) (a) Rinehart, J. D.; Long, J. R. Exploiting single-ion anisotropy in the design of f-element single-molecule magnets. *Chem. Sci.* **2011**, *2*, 2078−2085. (b) Sorace, L.; Benelli, C.; Gatteschi, D. Lanthanides in molecular magnetism: old tools in a new field. *Chem. Soc. Rev.* **2011**, *40*, 3092−3104.

(4) (a) Gatteschi, D.; Sessoli, R.; Villain, J. *Molecular Nanomagnets*; Oxford University Press: Oxford, U.K., 2006. (b) Gatteschi, D. Molecular Magnetism: A basis for new materials. *Adv. Mater.* **1994**, *6*, 635−645.

(5) (a) Molecular spintronics and quantum computing. *J. Mater. Chem.* **2009**, *19*, 1670−1671.10.1039/b901955n (b) Leuenberger, M. N.; Loss, D. Quantum computing in molecular magnets. *Nature* **2001**, *410*, 789−793.

(6) Bogani, L.; Wernsdorfer, W. Molecular spintronics using single-molecule magnets. *Nat. Mater.* **2008**, *7*, 179−186.

(7) (a) Blagg, R. J.; Muryn, C. A.; McInnes, E. J. L.; Tuna, F.; Winpenny, R. E. P. Single Pyramid Magnets: Dy_5 Pyramids with Slow Magnetic Relaxation to 40 K. *Angew. Chem., Int. Ed.* **2011**, *50*, 6530−6533. (b) Blagg, R. J.; Tuna, F.; McInnes, E. J. L.; Winpenny, R. E. P. Pentametallic lanthanide-alkoxide square-based pyramids: high energy barrier for thermal relaxation in a holmium single molecule magnet. *Chem. Commun.* **2011**, *47*, 10587−10589. (c) Hewitt, I. J.; Tang, J.; Madhu, N. T.; Anson, C. E.; Lan, Y.; Luzon, J.; Etienne, M.; Sessoli, R.; Powell, A. K. Coupling Dy_3 Triangles Enhances Their Slow Magnetic Relaxation. *Angew. Chem., Int. Ed.* **2010**, *49*, 6352−6356. (d) Lin, P.-H.; Burchell, T. J.; Ungur, L.; Chibotaru, L. F.; Wernsdorfer, W.; Murugesu, M. A Polynuclear Lanthanide Single-Molecule Magnet with a Record Anisotropic Barrier. *Angew. Chem., Int. Ed.* **2009**, *48*, 9489−9492. (e) Liu, J.; Chen, Y.-C.; Liu, J.-L.; Vieru, V.; Ungur, L.; Jia, J.-H.; Chibotaru, L. F.; Lan, Y.; Wernsdorfer, W.; Gao, S.; Chen, X.-M.; Tong, M.-L. A Stable Pentagonal Bipyramidal Dy(III) Single-Ion Magnet with a Record Magnetization Reversal Barrier over 1000 K. *J. Am. Chem. Soc.* **2016**, *138*, 5441−5450. (f) Blagg, R. J.; Ungur, L.; Tuna, F.; Speak, J.; Comar, P.; Collison, D.; Wernsdorfer, W.; McInnes, E. J. L.; Chibotaru, L. F.; Winpenny, R. E. P. Magnetic relaxation pathways in lanthanide single-molecule magnets. *Nat. Chem.* **2013**, *5*, 673−678.

(8) Milios, C. J.; Vinslava, A.; Wernsdorfer, W.; Moggach, S.; Parsons, S.; Perlepes, S. P.; Christou, G.; Brechin, E. K. A Record Anisotropy Barrier for a Single-Molecule Magnet. *J. Am. Chem. Soc.* **2007**, *129*, 2754−2755.

(9) (a) Rinehart, J. D.; Fang, M.; Evans, W. J.; Long, J. R. A N_2^{3-} Radical-Bridged Terbium Complex Exhibiting Magnetic Hysteresis at 14 K. *J. Am. Chem. Soc.* **2011**, *133*, 14236−14239. (b) Rinehart, J. D.; Fang, M.; Evans, W. J.; Long, J. R. Strong exchange and magnetic blocking in N_2^{3-}radical-bridged lanthanide complexes. *Nat. Chem.* **2011**, *3*, 538−542.

(10) Gupta, S. K.; Rajeshkumar, T.; Rajaraman, G.; Murugavel, R. An air-stable Dy(iii) single-ion magnet with high anisotropy barrier and blocking temperature. *Chem. Sci.* **2016**, *7*, 5181−5191.

(11) (a) Langley, S. K.; Moubaraki, B.; Murray, K. S. A heptadecanuclear $Mn^{III}_9Dy^{III}_8$ cluster derived from triethanolamine with two edge sharing supertetrahedra as the core and displaying SMM behaviour. *Dalton Trans.* **2010**, *39*, 5066−5069. (b) Rigaux, G.; Inglis, R.; Morrison, S.; Prescimone, A.; Cadiou, C.; Evangelisti, M.; Brechin, E. K. Enhancing Ueff in oxime-bridged $[Mn^{III}_6Ln^{III}_2]$ hexagonal prisms. *Dalton Trans.* **2011**, *40*, 4797−4799.

(12) (a) Langley, S. K.; Wielechowski, D. P.; Moubaraki, B.; Murray, K. S. Enhancing the magnetic blocking temperature and magnetic coercivity of $\{Cr^{III}_2Ln^{III}_2\}$ single-molecule magnets via bridging ligand modification. *Chem. Commun.* **2016**, *52*, 10976−10979. (b) Langley, S. K.; Wielechowski, D. P.; Vieru, V.; Chilton, N. F.; Moubaraki, B.; Abrahams, B. F.; Chibotaru, L. F.; Murray, K. S. A $\{Cr^{III}_2Dy^{III}_2\}$ Single-Molecule Magnet: Enhancing the Blocking Temperature through 3d Magnetic Exchange. *Angew. Chem., Int. Ed.* **2013**, *52*, 12014−12019.

(13) Schray, D.; Abbas, G.; Lan, Y.; Mereacre, V.; Sundt, A.; Dreiser, J.; Waldmann, O.; Kostakis, G. E.; Anson, C. E.; Powell, A. K. Magnetische Suszeptibilitätsmessung und ^{57}Fe-Mößbauer- Spektroskopie an einem ferromagnetischen $Fe^{III}_4Dy_4$-Ring. *Angew. Chem.* **2010**, *122*, 5312−5315.

(14) (a) Li, M.; Ako, A. M.; Lan, Y.; Wernsdorfer, W.; Buth, G.; Anson, C. E.; Powell, A. K.; Wang, Z.; Gao, S. New heterometallic $[Mn^{III}_4Ln^{III}_4]$ wheels incorporating formate ligands. *Dalton Trans.* **2010**, *39*, 3375−3377. (b) Li, M.; Lan, Y.; Ako, A. M.; Wernsdorfer, W.; Anson, C. E.; Buth, G.; Powell, A. K.; Wang, Z.; Gao, S. A Family of 3d-4f Octa-Nuclear $[Mn^{III}_4Ln^{III}_4]$ Wheels (Ln = Sm, Gd, Tb, Dy, Ho, Er, and Y): Synthesis, Structure, and Magnetism. *Inorg. Chem.* **2010**, *49*, 11587−11594. (c) Vignesh, K. R.; Langley, S. K.; Moubaraki, B.; Murray, K. S.; Rajaraman, G. Large Hexadecametallic $\{Mn^{III}–Ln^{III}\}$ Wheels: Synthesis, Structural, Magnetic, and Theoretical Characterization. *Chem. - Eur. J.* **2015**, *21*, 16364−16369.

(15) (a) Ahmed, N.; Das, C.; Vaidya, S.; Langley, S. K.; Murray, K. S.; Shanmugam, M. Nickel(II)−Lanthanide(III) Magnetic Exchange Coupling Influencing Single-Molecule Magnetic Features in $\{Ni_2Ln_2\}$ Complexes. *Chem. - Eur. J.* **2014**, *20*, 14235−14239. (b) Chandrasekhar, V.; Bag, P.; Kroener, W.; Gieb, K.; Müller, P. Pentanuclear Heterometallic $\{Ni_2Ln_3\}$ (Ln = Gd, Dy, Tb, Ho) Assemblies. Single-Molecule Magnet Behavior and Multistep Relaxation in the Dysprosium Derivative. *Inorg. Chem.* **2013**, *52*, 13078−13086.

(16) (a) Oyarzabal, I.; Ruiz, J.; Ruiz, E.; Aravena, D.; Seco, J. M.; Colacio, E. Increasing the effective energy barrier promoted by the change of a counteranion in a Zn-Dy-Zn SMM: slow relaxation via the second excited state. *Chem. Commun.* **2015**, *51*, 12353−12356. (b) Costes, J. P.; Titos-Padilla, S.; Oyarzabal, I.; Gupta, T.; Duhayon, C.; Rajaraman, G.; Colacio, E. Analysis of the Role of Peripheral Ligands Coordinated to Zn^{II} in Enhancing the Energy Barrier in Luminescent Linear Trinuclear Zn-Dy-Zn Single-Molecule Magnets. *Chem. - Eur. J.* **2015**, *21*, 15785−15796. (c) Costes, J. P.; Titos-Padilla, S.; Oyarzabal, I.; Gupta, T.; Duhayon, C.; Rajaraman, G.; Colacio, E. Effect of Ligand Substitution around the Dy^{III} on the SMM Properties of Dual-Luminescent Zn−Dy and Zn−Dy−Zn Complexes with Large Anisotropy Energy Barriers: A Combined Theoretical and Experimental Magnetostructural Study. *Inorg. Chem.* **2016**, *55*, 4428−4440. (d) Upadhyay, A.; Singh, S. K.; Das, C.; Mondol, R.; Langley, S. K.; Murray, K. S.; Rajaraman, G.; Shanmugam, M. Enhancing the effective energy barrier of a Dy(iii) SMM using a bridged diamagnetic Zn(ii) ion. *Chem. Commun.* **2014**, *50*, 8838−8841.

DOI: 10.1021/acs.inorgchem.6b02720
Inorg. Chem. 2017, 56, 2518−2532

(17) (a) Langley, S. K.; Chilton, N. F.; Moubaraki, B.; Murray, K. S. Anisotropy barrier enhancement via ligand substitution in tetranuclear $\{Co^{III}_2Ln^{III}_2\}$ single molecule magnets. *Chem. Commun.* **2013**, *49*, 6965−6967. (b) Langley, S. K.; Chilton, N. F.; Moubaraki, B.; Murray, K. S. Single-Molecule Magnetism in Three Related $\{Co^{III}_2Dy^{III}_2\}$-Acetylacetonate Complexes with Multiple Relaxation Mechanisms. *Inorg. Chem.* **2013**, *52*, 7183−7192. (c) Langley, S. K.; Chilton, N. F.; Moubaraki, B.; Murray, K. S. Single-molecule magnetism in $\{Co^{III}_2Dy^{III}_2\}$-amine-polyalcohol-acetylacetonate complexes: effects of ligand replacement at the Dy^{III} sites on the dynamics of magnetic relaxation. *Inorg. Chem. Front.* **2015**, *2*, 867−875. (d) Langley, S. K.; Chilton, N. F.; Ungur, L.; Moubaraki, B.; Chibotaru, L. F.; Murray, K. S. Heterometallic Tetranuclear $[Ln^{III}_2Co^{III}_2]$ Complexes Including Suppression of Quantum Tunneling of Magnetization in the $[Dy^{III}_2Co^{III}_2]$ Single Molecule Magnet. *Inorg. Chem.* **2012**, *51*, 11873−11881. (e) Langley, S. K.; Ungur, L.; Chilton, N. F.; Moubaraki, B.; Chibotaru, L. F.; Murray, K. S. Single-Molecule Magnetism in a Family of $\{Co^{III}_2Dy^{III}_2\}$ Butterfly Complexes: Effects of Ligand Replacement on the Dynamics of Magnetic Relaxation. *Inorg. Chem.* **2014**, *53*, 4303−4315.

(18) Cowieson, N. P.; Aragao, D.; Clift, M.; Ericsson, D. J.; Gee, C.; Harrop, S. J.; Mudie, N.; Panjikar, S.; Price, J. R.; Riboldi-Tunnicliffe, A.; Williamson, R.; Caradoc-Davies, T. MX1: a bending-magnet crystallography beamline serving both chemical and macromolecular crystallography communities at the Australian Synchrotron. *J. Synchrotron Radiat.* **2015**, *22*, 187−190.

(19) McPhillips, T. M.; McPhillips, S. E.; Chiu, H.-J.; Cohen, A. E.; Deacon, A. M.; Ellis, P. J.; Garman, E.; Gonzalez, A.; Sauter, N. K.; Phizackerley, R. P.; Soltis, S. M.; Kuhn, P. Blu-Ice and the Distributed Control System: software for data acquisition and instrument control at macromolecular crystallography beamlines. *J. Synchrotron Radiat.* **2002**, *9*, 401−406.

(20) Kabsch, W. Automatic processing of rotation diffraction data from crystals of initially unknown symmetry and cell constants. *J. Appl. Crystallogr.* **1993**, *26*, 795−800.

(21) Sheldrick, G. A short history of SHELX. *Acta Crystallogr., Sect. A: Found. Crystallogr.* **2008**, *64*, 112−122.

(22) Sheldrick, G. M. *SHELXL-97, Programs for X-ray Crystal Structure Refinement*; University of Göttingen, Göttingen, Germany, 1997.

(23) Barbour, L. J. *J. Supramol. Chem.* **2001**, *1*, 189−191.

(24) Aquilante, F.; Pedersen, T. B.; Veryazov, V.; Lindh, R. MOLCAS—a software for multiconfigurational quantum chemistry calculations. *WIREs Comput. Mol. Sci.* **2013**, *3*, 143−149.

(25) Hess, B. A.; Marian, C. M.; Wahlgren, U.; Gropen, O. A mean-field spin-orbit method applicable to correlated wavefunctions. *Chem. Phys. Lett.* **1996**, *251*, 365−371.

(26) Roos, B. O.; Malmqvist, P.-A. Relativistic quantum chemistry: the multiconfigurational approach. *Phys. Chem. Chem. Phys.* **2004**, *6*, 2919−2927.

(27) Roos, B. O.; Lindh, R.; Malmqvist, P.-A.; Veryazov, V.; Widmark, P.-O.; Borin, A. C. New Relativistic Atomic Natural Orbital Basis Sets for Lanthanide Atoms with Applications to the Ce Diatom and LuF_3. *J. Phys. Chem. A* **2008**, *112*, 11431−11435.

(28) Malmqvist, P. A.; Roos, B. O.; Schimmelpfennig, B. The restricted active space (RAS) state interaction approach with spin-orbit coupling. *Chem. Phys. Lett.* **2002**, *357*, 230−240.

(29) Chibotaru, L. F.; Ungur, L. Ab initio calculation of anisotropic magnetic properties of complexes. I. Unique definition of pseudospin Hamiltonians and their derivation. *J. Chem. Phys.* **2012**, *137*, 064112−22.

(30) Chibotaru, L. F.; Ungur, L. *Program POLY_ANISO*; University of Leuven, Leuven, Belgium, 2006.

(31) Noodleman, L. Valence bond description of antiferromagnetic coupling in transition metal dimers. *J. Chem. Phys.* **1981**, *74*, 5737−5743.

(32) (a) Christian, P.; Rajaraman, G.; Harrison, A.; Helliwell, M.; McDouall, J. J. W.; Raftery, J.; Winpenny, R. E. P. Synthesis and studies of a trinuclear Mn(ii) carboxylate complex. *Dalton Trans.* **2004**, 2550−2555. (b) Piligkos, S.; Rajaraman, G.; Soler, M.; Kirchner, N.; van Slageren, J.; Bircher, R.; Parsons, S.; Gudel, H.-U.; Kortus, J.; Wernsdorfer, W.; Christou, G.; Brechin, E. K. Studies of an Enneanuclear Manganese Single-Molecule Magnet. *J. Am. Chem. Soc.* **2005**, *127*, 5572−5580. (c) Rajaraman, G.; Cano, J.; Brechin, E. K.; McInnes, E. J. L. Density functional calculations of a tetradecametallic iron(iii) cluster with a very large spin ground state. *Chem. Commun.* **2004**, 1476−1477. (d) Ruiz, E.; Cano, J.; Alvarez, S.; Alemany, P. Broken symmetry approach to calculation of exchange coupling constants for homobinuclear and heterobinuclear transition metal complexes. *J. Comput. Chem.* **1999**, *20*, 1391−1400. (e) Ruiz, E.; Cano, J.; Alvarez, S.; Caneschi, A.; Gatteschi, D. Theoretical Study of the Magnetic Behavior of Hexanuclear Cu(II) and Ni(II) Polysiloxanolato Complexes. *J. Am. Chem. Soc.* **2003**, *125*, 6791−6794. (f) Ruiz, E.; Rodríguez-Fortea, A.; Cano, J.; Alvarez, S.; Alemany, P. About the calculation of exchange coupling constants in polynuclear transition metal complexes. *J. Comput. Chem.* **2003**, *24*, 982−989.

(33) (a) Berg, N.; Hooper, T. N.; Liu, J.; Beedle, C. C.; Singh, S. K.; Rajaraman, G.; Piligkos, S.; Hill, S.; Brechin, E. K.; Jones, L. F. Synthetic, structural, spectroscopic and theoretical study of a Mn(iii)-Cu(ii) dimer containing a Jahn-Teller compressed Mn ion. *Dalton Trans.* **2013**, *42*, 207−216. (b) Berg, N.; Rajeshkumar, T.; Taylor, S. M.; Brechin, E. K.; Rajaraman, G.; Jones, L. F. What Controls the Magnetic Interaction in bis-μ-Alkoxo Mn^{III} Dimers? A Combined Experimental and Theoretical Exploration. *Chem. - Eur. J.* **2012**, *18*, 5906−5918. (c) Ghosh, S.; Singh, S. K.; Tewary, S.; Rajaraman, G. Enhancing the double exchange interaction in a mixed valence $\{V^{III}$-$V^{II}\}$ pair: a theoretical perspective. *Dalton Trans.* **2013**, *42*, 16490−16493. (d) Rajaraman, G.; Murugesu, M.; Sanudo, E. C.; Soler, M.; Wernsdorfer, W.; Helliwell, M.; Muryn, C.; Raftery, J.; Teat, S. J.; Christou, G.; Brechin, E. K. A Family of Manganese Rods: Syntheses, Structures, and Magnetic Properties. *J. Am. Chem. Soc.* **2004**, *126*, 15445−15457.

(34) (a) Baker, M. L.; Timco, G. A.; Piligkos, S.; Mathieson, J. S.; Mutka, H.; Tuna, F.; Kozlowski, P.; Antkowiak, M.; Guidi, T.; Gupta, T.; Rath, H.; Woolfson, R. J.; Kamieniarz, G.; Pritchard, R. G.; Weihe, H.; Cronin, L.; Rajaraman, G.; Collison, D.; McInnes, E. J. L.; Winpenny, R. E. P. A classification of spin frustration in molecular magnets from a physical study of large odd-numbered-metal, odd electron rings. *Proc. Natl. Acad. Sci. U. S. A.* **2012**, *109*, 19113−19118. (b) Christian, P.; Rajaraman, G.; Harrison, A.; McDouall, J. J. W.; Raftery, J. T.; Winpenny, R. E. P. Structural, magnetic and DFT studies of a hydroxide-bridged $\{Cr_8\}$ wheel. *Dalton Trans.* **2004**, 1511−1512. (c) Cremades, E.; Cano, J.; Ruiz, E.; Rajaraman, G.; Milios, C. J.; Brechin, E. K. Theoretical Methods Enlighten Magnetic Properties of a Family of Mn_6 Single-Molecule Magnets. *Inorg. Chem.* **2009**, *48*, 8012−8019. (d) Vignesh, K. R.; Langley, S. K.; Murray, K. S.; Rajaraman, G. What Controls the Magnetic Exchange Interaction in Mixed- and Homo-Valent Mn_7 Disc-Like Clusters? A Theoretical Perspective. *Chem. - Eur. J.* **2015**, *21*, 2881−2892.

(35) Becke, A. D. Density functional thermochemistry. III. The role of exact exchange. *J. Chem. Phys.* **1993**, *98*, 5648−5652.

(36) Frisch, M. J.; Trucks, G. W.; Schlegel, H. B.; Scuseria, G. E.; Robb, M. A.; Cheeseman, J. R.; Scalmani, G.; Barone, V.; Mennucci, B.; Petersson, G. A.; Nakatsuji, H.; Caricato, M.; Li, X.; Hratchian, H. P.; Izmaylov, A. F.; Bloino, J.; Zheng, G.; Sonnenberg, J. L.; Hada, M.; Ehara, M.; Toyota, K.; Fukuda, R.; Hasegawa, J.; Ishida, M.; Nakajima, T.; Honda, Y.; Kitao, O.; Nakai, H.; Vreven, T.; Montgomery, J. A., Jr.; Ogliaro, F.; Bearpark, M.; Heyd, J. J.; Brothers, E.; Kudin, K. N.; Staroverov, V. N.; Kobayashi, R.; Normand, J.; Raghavachari, K.; Rendell, A.; Burant, J. C.; Iyengar, S. S.; Tomasi, J.; Cossi, M.; Rega, N.; Millam, J. M.; Klene, M.; Knox, J. E.; Cross, J. B.; Bakken, V.; Adamo, C.; Jaramillo, J.; Gomperts, R.; Stratmann, R. E.; Yazyev, O.; Austin, A. J.; Cammi, R.; Pomelli, C.; Ochterski, J. W.; Martin, R. L.; Morokuma, K.; Zakrzewski, V. G.; Voth, G. A.; Salvador, P.; Dannenberg, J. J.; Dapprich, S.; Daniels, A. D.; Farkas, Ö.; Foresman, J. B.; Ortiz, J. V.; Cioslowski, J. A.; Fox, D. J. *Gaussian 09, R. A.02*; Wallingford, CT, 2009.

DOI: 10.1021/acs.inorgchem.6b02720
Inorg. Chem. 2017, 56, 2518−2532

(37) Cundari, T. R.; Stevens, W. J. Effective core potential methods for the lanthanides. *J. Chem. Phys.* **1993**, *98*, 5555−5565.
(38) (a) Schaefer, A.; Horn, H.; Ahlrichs, R. Fully optimized contracted Gaussian basis sets for atoms Li to Kr. *J. Chem. Phys.* **1992**, *97*, 2571−2577. (b) Schaefer, A.; Huber, C.; Ahlrichs, R. Fully optimized contracted Gaussian basis sets of triple zeta valence quality for atoms Li to Kr. *J. Chem. Phys.* **1994**, *100*, 5829−5835.
(39) Langley, S. K.; Le, C.; Ungur, L.; Moubaraki, B.; Abrahams, B. F.; Chibotaru, L. F.; Murray, K. S. Heterometallic 3d−4f Single-Molecule Magnets: Ligand and Metal Ion Influences on the Magnetic Relaxation. *Inorg. Chem.* **2015**, *54*, 3631−3642.
(40) (a) Cirera, J.; Ruiz, E.; Alvarez, S. Shape and Spin State in Four-Coordinate Transition-Metal Complexes: The Case of the d6 Configuration. *Chem. - Eur. J.* **2006**, *12*, 3162−3167. (b) Pinsky, M.; Avnir, D. Continuous Symmetry Measures. 5. The Classical Polyhedra. *Inorg. Chem.* **1998**, *37*, 5575−5582.
(41) Lucaccini, E.; Briganti, M.; Perfetti, M.; Vendier, L.; Costes, J.-P.; Totti, F.; Sessoli, R.; Sorace, L. Relaxation Dynamics and Magnetic Anisotropy in a Low-Symmetry Dy^{III} Complex. *Chem. - Eur. J.* **2016**, *22*, 5552−5562.
(42) (a) Feltham, H. L. C.; Klower, F.; Cameron, S. A.; Larsen, D. S.; Lan, Y.; Tropiano, M.; Faulkner, S.; Powell, A. K.; Brooker, S. A family of 13 tetranuclear zinc(ii)-lanthanide(iii) complexes of a [3 + 3] Schiff-base macrocycle derived from 1,4-diformyl-2,3-dihydroxybenzene. *Dalton Trans.* **2011**, *40*, 11425−11432. (b) Yamashita, A.; Watanabe, A.; Akine, S.; Nabeshima, T.; Nakano, M.; Yamamura, T.; Kajiwara, T. Wheel-Shaped $Er^{III}Zn^{II}_3$ Single-Molecule Magnet: A Macrocyclic Approach to Designing Magnetic Anisotropy. *Angew. Chem., Int. Ed.* **2011**, *50*, 4016−4019.
(43) Gupta, T.; Velmurugan, G.; Rajeshkumar, T.; Rajaraman, G. Role of Lanthanide-Ligand bonding in the magnetization relaxation of mononuclear single-ion magnets: A case study on Pyrazole and Carbene ligated Ln^{III} (Ln = Tb, Dy, Ho, Er) complexes. *J. Chem. Sci.* **2016**, *128*, 1615−1630.
(44) Lines, M. E. Orbital Angular Momentum in the Theory of Paramagnetic Clusters. *J. Chem. Phys.* **1971**, *55*, 2977−2984.
(45) (a) Zhou, Q.; Yang, F.; Liu, D.; Peng, Y.; Li, G.; Shi, Z.; Feng, S. Synthesis, Structures, and Magnetic Properties of Three Fluoride-Bridged Lanthanide Compounds: Effect of Bridging Fluoride Ions on Magnetic Behaviors. *Inorg. Chem.* **2012**, *51*, 7529−7536. (b) Pineda, E. M.; Chilton, N. F.; Marx, R.; Dörfel, M.; Sells, D. O.; Neugebauer, P.; Jiang, S.-D.; Collison, D.; Sclageren, J. V.; McInnes, E. J. L.; Winpenny, R. E. P. Direct measurement of dysprosium(III)···dysprosium(III) interactions in a single-molecule magnet. *Nat. Commun.* **2014**, *5*, 5243.
(46) (a) Yu, W.-R.; Lee, G.-H.; Yang, E.-C. Systematic studies of the structures and magnetic properties for a family of cubane complexes with the formula: $[M_2Ln_2]$ (Ln = Dy, Gd; M = Ni, Zn) and $[Ni_2Y_2]$. *Dalton Trans.* **2013**, *42*, 3941−3949. (b) Abtab, S. M. T.; Maity, M.; Bhattacharya, K.; Sañudo, E. C.; Chaudhury, M. Syntheses, Structures, and Magnetic Properties of a Family of Tetranuclear Hydroxido-Bridged $Ni^{II}_2Ln^{III}_2$ (Ln = La, Gd, Tb, and Dy) Complexes: Display of Slow Magnetic Relaxation by the Zinc(II)−Dysprosium(III) Analogue. *Inorg. Chem.* **2012**, *51*, 10211−10221. (c) Meng, Z.-S.; Guo, F.-S.; Liu, J.-L.; Leng, J.-D.; Tong, M.-L. Heterometallic cubane-like $\{M_2Ln_2\}$ (M = Ni, Zn; Ln = , Gd, Dy) and $\{Ni_2Y_2\}$ aggregates. Synthesis, structures and magnetic properties. *Dalton Trans.* **2012**, *41*, 2320−2329.

DOI: 10.1021/acs.inorgchem.6b02720
Inorg. Chem. 2017, 56, 2518−2532